**Glycoengineered keratinocyte library reveals essential functions of specific glycans for all stages of HSV-1 infection**

Running title: Different classes of glycans are essential for all stages of HSV-1 life cycle

Ieva Bagdonaite[1]*, Irina N Marinova[1], Asha M Rudjord-Levann[1], Emil MH Pallesen[1], Sarah King-Smith[1], Troels B Rømer[1], Yen-Hsi Chen[1], Sigvard Olofsson[2], Rickard Nordén[2], Tomas Bergström[2], Sally Dabelsteen[3] and Hans H Wandall[1]*

[1] Copenhagen Center for Glycomics, Institute of Cellular and Molecular Medicine, University of Copenhagen, DK-2200 Copenhagen, Denmark

[2] Department of Infectious Diseases, Institute of Biomedicine, University of Gothenburg, SE-41346 Gothenburg, Sweden

[3] School of Dentistry, University of Copenhagen, DK-2200 Copenhagen, Denmark

* Corresponding authors

E-mail: hhw@sund.ku.dk (HHW) and ieva@sund.ku.dk (IB)

**Abstract**

Viral and host glycans represent an understudied aspect of host-pathogen interactions, despite potential implications for treatment of viral infections. This is due to lack of easily accessible tools for analyzing glycan function in a meaningful context. Here we generated a glycoengineered keratinocyte library delineating human glycosylation pathways to uncover roles of specific glycans at different stages of herpes simplex virus type 1 (HSV-1) infectious cycle. We show the importance of cellular glycosaminoglycans and glycosphingolipids for HSV-1 attachment, N-glycans for entry and spread, and O-glycans for propagation. While altered virion surface structures had minimal effects on the early interactions with wild type cells, mutation of specific O-glycosylation sites affected glycoprotein surface expression and function. In conclusion, the data demonstrates the importance of specific glycans in a clinically relevant human model of HSV-1 infection and highlights the utility of genetic engineering to elucidate the roles of specific viral and cellular carbohydrate structures.

## Introduction

Upon infection of human cells with enveloped viruses, the virus hijacks the secretory pathway leading to the decoration of the newly formed viral proteins and membranes with host glycans. The resulting glycans influence several aspects of viral biology, with the most appreciated function being immunological shields that prevent the immune system from recognizing the viral particles [1]. However, other functions of the abundantly present cellular and viral glycans are still underexplored mainly because of the lack of accessible tools and model systems.

Glycosylation is among the most diverse post-translational modifications, dynamically shaping the glycans on proteins and lipids traveling through the secretory pathway, and comprising an extensive glycocalyx on the cell surface. There are three major classes of cell surface glycoconjugates – glycoproteins, glycosphingolipids (GSLs) and proteoglycans carrying long glycosaminoglycan (GAG) chains – that all carry out numerous functions, including fine-tuning of molecular interactions, intra- and intercellular communications, and immune modulation [2-4]. Due to non-template driven synthesis and the resulting heterogeneity it is methodologically challenging to investigate the functions of specific glycans in biological systems. We have recently generated glycoengineered cell libraries by CRISPR/Cas9 gene editing composed of cells lacking different glycosyltransferases delineating human glycosylation pathways to dissect the importance of glycosylation in cell and molecular biology [5-8].

Here we used herpes simplex virus type 1 (HSV-1) as a model to systematically assess the importance of specific glycans in infection of a relevant human cellular system – the skin. We generated glycoengineered HaCaT keratinocytes by introducing targeted deletions in the cellular glycome, including select initiation, branching and capping events, and encompassing all the major classes of glycocojungates (Figure 1A). The use of live virus in a natural target cell, representing the primary site of infection, allowed us both to examine isolated viral life cycle events, such as binding, entry, propagation, and spread, and follow viral spread in 3D differentiated skin tissue models built with the glycoengineered cells.

HSV-1 is a widespread human pathogen persisting in sensory neurons for a lifetime and causing recurrent cutaneous lesions due to reactivation [9]. Importantly, it can cause life-threatening CNS complications, which is a major risk for both immunocompetent and immunocompromised

individuals, and may predispose to neurodegenerative disease [10-12]. HSV-1 is a large dsDNA enveloped virus, encoding 12 surface glycoproteins important for viral entry, particle formation, and cell-to-cell spread [13, 14]. HSV-1 glycoproteins are confirmed to acquire both N-linked and mucin type O-linked glycans, and we have previously demonstrated the importance of elongated O-linked glycans for HSV-1 propagation [15-20]. On the host side, HSV-1 interacts with several cellular receptors including nectin-1, herpes virus entry mediator (HVEM), 3-O-sulfated heparan sulfate, integrins, and paired immunoglobulin-like receptor alpha (PILRα), which can be engaged by gD, gB or gH/gL [21-25]. The impact of glycans on the cellular receptors and the viral envelope proteins in modulating the distinct interactions are underexplored. Furthermore, while the importance of GAGs for HSV-1 initial attachment is well documented [26, 27], little is known about the role of GSLs.

To identify specific glycan structures important in HSV-1 biology, we analyzed isolated life cycle events using the library of glycoengineered cells. We find that each individual type of glycoconjugate affects at least one stage of HSV-1 life cycle and identify the critical glycan biosynthesis steps. We furthermore addressed roles of specific O-glycan acceptor amino acids on viral entry mediator gD and conserved fusogen gB. The work identifies the glycosylation steps that are essential for proper viral functions defining the scope of future mechanistic studies, but also suggests that local targeting of host glycosylation pathways by inhibitors or mimetics may be sufficient to inhibit redundant viral entry mechanisms.

## Results

### Generation of a glycogene knock out library in HaCaT keratinocytes

HaCaT is a human keratinocyte cell line capable of forming a stratified squamous epithelium, and thus allows evaluating the infection of the skin tropic HSV-1 in both cell and organotypic tissue culture. In order to address the role of specific glycan structures in the HSV-1 infectious cycle, we used precise gene editing to target glycosyltransferases involved in the early steps of core structure synthesis, and in major elongation and branching steps of the main glycosylation pathways, including N-linked glycosylation, mucin type O-linked glycosylation, as well as glycosphingolipid and glycosaminoglycan synthesis (Figure 1A, Table S1).

For N-linked glycans we generated *MGAT1*, *MGAT4A*, *MGAT4B*, *MGAT5*, and *MGAT5+4B* knock outs (KO). MGAT1 adds the first N-acetylglucosamine to the C-2 of core α3-linked mannose, and lack of this enzyme results in elimination of all N-glycan maturation steps, yielding high-mannose type N-glycans as confirmed by MS-glycoprofiling (Figure 1A, Figure S1). MGAT4A, MGAT4B and MGAT5 are responsible for N-glycan branching, where MGAT4A or MGAT4B initiate a β4-linked antenna on the α3-linked mannose, and MGAT5 performs β6-linked branching from the core α6-linked mannose. Lack of MGAT5 results in loss of tetra-antennary N-glycans, and loss of MGAT4 isoforms also strongly diminishes the content of tetra-antennary N-glycans (Figure S1). In addition, KO of each of the three branching enzymes resulted in increased relative abundance of hybrid type N-glycans, whereas double KO of *MGAT5* and *MGAT4B* increased the relative abundance of biantennary glycans (Figure S1).

For mucin type O-linked glycans, we knocked out core 1 synthase (*C1GALT1*), its obligate chaperone COSMC (*C1GALT1C1*), core 2 synthase (*GCNT1*), as well as the major core 1-capping glycosyltransferase *ST3GAL1*. Loss of C1GALT1 or COSMC eliminates the β3-linked galactose (core 1 structure), results in truncation of O-linked glycans to the initiating α-GalNAc, and prevents assembly on secreted α-benzyl GalNAc precursor used in CORA O-glycoprofiling (Figure 1A, Figure S2). GCNT1 is the predominant enzyme creating the branched core 2 structure by addition of β6-linked GlcNAc to the GalNAc. Loss of GCNT1 nearly abolished all the disialylated core 2 structures, though some structures matching the composition of monosialylated core 2 could still be detected. Such structures cannot be discriminated from isobaric core 1 structures, and a minor contribution from other GCNTs to core 2 synthesis cannot be excluded either. Finally, loss of ST3GAL1 significantly reduces the α3-linked sialic acid content and results in predominantly non-capped core 1 structures (Figure S2). We also targeted the synthesis of GSLs and GAGs. Through KO of *B4GALT5* or *ST3GAL5*, which represent non-redundant steps of GM3 glycosphingolipid synthesis, we generated cells with the truncated GSLs, glucosylceramide (GlcCer) and lactosylceramide (LacCer), respectively (Figure 1A). Furthermore, we knocked out *B4GALT7*, which adds a β4-linked galactose to the initiating xylose in GAG biosynthesis, effectively truncating all classes of GAGs on membrane proteoglycans (Figure 1A). The generated keratinocyte library represents a screening platform for roles of defined cell-surface presented glycan structures in HSV-1 biology in the context of natural infection.

**Propagation of HSV-1 in glycoengineered keratinocytes**

To define the capacity of HSV-1 to complete the infectious cycle in glycoengineered keratinocytes, we infected confluent monolayers of the KO cell lines with HSV-1, and quantified HSV-1 DNA and infectious particles in the growth media at 17 hours post infection (hpi) by qPCR and plaque titration, respectively. As a measure for viral replication fitness, we calculated the ratio of genome copies/infectious particles for each KO. When infecting cells with truncated O-glycans (*C1GALT1* and *C1GALT1C1* KOs) a decrease in titers was detected (Figure 1B). In contrast, the same cells generated close to normal levels of viral DNA (Figure 1C), suggesting decreased fitness of virions lacking elongated O-glycans (Figure 1D). Looking into sialylated core 1 O-glycans, we found a trend towards accelerated production of viral particles in cells deficient in O-glycan sialylation (*ST3GAL1* KO). As the viral particles from these KO cells displayed normal fitness characteristics, the data indicate that each step of the O-glycan machinery has a distinct role in virus production and maturation. In cells lacking N-glycan maturation (*MGAT1* KO) we also found a lower number of infectious particles with an apparent decreased fitness as indicated by an increase in the ratio of DNA/infectious particles (Figure 1D). Interestingly, this was different in cell lines lacking the β6-antennae on N-glycans (*MGAT5*, *MGAT5+4B*) where we found that a higher proportion of progeny virions were infectious, suggesting increased fitness (Figure 1D). When analysing cells with glycosphingolipid synthesis defects, we found that while lack of LacCer sialylation (*ST3GAL5* KO) accelerated virus production, no changes were observed in viral fitness. In contrast, truncation to GlcCer (*B4GALT5* KO) did not affect viral propagation dynamics (Figure 1D-F). Finally, we found that truncation of cellular glycosaminoglycans (GAGs) also increased the production of viral particles, though with a slight decrease in viral fitness (Figure 1D-F). In conclusion, apart from substantial loss of titers in cells bearing truncated O-glycans, most of the tested glycogene disruptions permitted HSV-1 replication. We next evaluated the impact of defined glycan classes to distinct stages of the HSV-1 infectious cycle, including binding and entry, viral assembly and properties of progeny virus, and cell-to-cell spread.

**Binding and entry of HSV-1 to mutant cell lines**

HSV-1 binds and enters human keratinocytes very rapidly, with around 30 % of virions bound after 20 min on ice, 80 % after 2 hours and complete binding after 3 hours [28]. Most of the bound virions enter keratinocytes within 5 min after warming [28]. Perturbations in each of the investigated glycosylation pathways modulated early virus-host interactions (Figure 2A-C). Cells lacking core 1 O-glycan sialylation (*ST3GAL1* KO) showed reduced binding (Figure 2A, 2B), which was also reflected in the subsequent entry experiments (Figure 2D, 2E). In contrast, diminished core 2 O-glycan branching resulted in increased binding (Figure 2A, 2B). Lack of complex N-glycans and reduced β4-antenna branching (*MGAT1* KO and *MGAT4B* KO) showed reduced binding, again also reflected in the entry experiments (Figure 2D, 2E). Interestingly, deletion of *MGAT4A*, another isoform catalysing the β4-antenna synthesis on N-glycans, likely on another subset of proteins or sites in proteins [29, 30], selectively affected viral entry (Figure 2E). Cells displaying truncated glycolipids showed a reduction in binding to around 50 % of that of WT (Figure 2A, 2B). A similar effect was observed in both *B4GALT5* and *ST3GAL5* KOs, controlling the consecutive steps in the biosynthesis of the glycosphingolipid GM3. In addition, an incremental reduction in entry was observed for *B4GALT5* KO cells, suggesting involvement of glycolipids in both viral binding and entry to host cells (Figure 2D, 2E).

Then, we analysed cells impaired in GAG biosynthesis, and found an almost complete loss of binding to cells presenting only the initiating xylose on proteoglycans (*B4GALT7* KO). This fits well with the known importance of heparan sulfate (HS) in the initial attachment of HSV-1 (Figure 2A, 2B) [26], although we still lack a clear understanding of finer structural requirements of GAGs presented on their core proteins in the context of total cellular glycome. Therefore, to further dissect the importance of GAG binding determinants we used recombinant HSV-1 gC, limiting the interactions to a single viral protein known to bind to synthetic GAGs *in vitro*, similarly to intact HSV-1 [27, 31, 32]. As expected, no binding was detected on *B4GALT7* KO cells (Figure 2F), and to further confirm the selectivity for HS we treated HaCaT WT cells with heparinases 1, 2, and 3. Loss of HS completely abolished gC binding suggesting minimal interaction with chondroitin sulfate (CS) or dermatan sulfate (DS) presented on the cell surface (Figure 2F). Minimal changes in cell staining for bound HSV-1 gC after chondroitinase ABC treatment further supported this interpretation. Next, we analyzed a library of glycoengineered CHO cells delineating the GAG biosynthesis pathways (Figure 2G) and quantified gC binding by flow cytometry (Figure 2H) [33]. This library

included selective elimination of HS or CS (*Extl2* + *Extl3* KO and *Csgalnact1* KO + *Csgalnact2* KO + *Chsy1* KO, respectively), reduction in chain polymerization of HS or CS (*Ext1* KO + *Ext2* KO and *Chpf* KO, respectively), elimination of HS N-sulfation, also effectively diminishing follow-up O-sulfation (*Ndst1* KO + *Ndst2* KO), as well as elimination of 4-O sulfation of CS and DS units of CS chains (*Chst11* KO + *Chst12* KO + *Chst13* KO + *Chst14* KO). In addition, we used *B4galt7* KO and *B3gat3* KO cells to truncate all GAGs to the initiating xylose and a short linker trisaccharide, respectively (Figure 2G). In agreement with the HaCaT cell staining data, manipulation of HS synthesis and chain length substantially decreased gC binding showing that the interaction was entirely dependent on HS sulfation and not compensated by the presence of CS (Figure 2H). Accordingly, manipulation of CS synthesis only slightly decreased gC binding independent of the predominant 4-O sulfation (Figure 2H). As expected, truncation to the linker also eliminated gC binding (Figure 2H). To our surprise, some binding was retained upon complete GAG truncation, possibly representing unspecific binding due to gross changes in the glycocalyx. In conclusion, by using cell surface presented GAGs, we were able to identify sulfated HS as the major contributor to HSV-1 gC binding and show that CS sulfation is not necessary for interaction with CS, at least in the presence of HS. More generally, the binding and entry assays show that perturbations in the cellular glycome landscape have immediate effects to early virus-cell interactions, which can be further dissected as demonstrated for the interaction between gC and HS.

**Viral assembly and properties of progeny virus**

We next investigated late stages of viral replication in KO cells with changes in protein glycosylation capacity and altered viral propagation dynamics. We probed the expression of gD and gB that promote virion envelopment. In WT most of gD signal was confined to the cell surface, partially overlapping with E-cadherin (Figure 3A), while gB primarily localized to the perinuclear compartment and secondary envelopment sites with some surface presentation, consistent with the literature (Figure 3B) [34]. In contrast, *C1GALT1C1* KO, *C1GALT1* KO, and *MGAT1* KO cells exhibited a weaker and more disperse gD immunostaining pattern with partial cytoplasmic accumulation suggesting issues with envelope glycoprotein trafficking (Figure 3A). In addition, gB exhibited poorer surface and perinuclear localization and presented in large clusters within the cells (Figure 3B). *ST3GAL1* KO cells displayed similar gB staining as WT (Figure 3B), while exhibiting

stronger gD signal (Figure 3A), which could explain accelerated virion production. Overall, the results suggest that lack of core 1 O-glycans or mature N-glycans causes defects in viral particle formation due to suboptimal incorporation of viral proteins, which would fit with the observed diminished titers or loss of fitness. In addition, using an HSV-1 strain with GFP-labelled capsid protein VP26 allowed us to observe differences in the localization of viral capsids. The capsids were found in nuclear assembly compartments, outer nuclear rim, and transitioning through the cytosol in WT and *ST3GAL1* KO cells. We observed lower numbers of capsid assembly sites in the nucleus and rare association with the outer nuclear rim in *C1GALT1C1* KO, *C1GALT1* KO and *MGAT1* KO cells, with the most pronounced effect in *C1GALT1C1* KO (Figure 3A, 3B).

We further explored the viral replication dynamics in WT and *C1GALT1C1* KO cells by live imaging of GFP-labelled HSV-1. Features seen in thin optical sections (Figure 3A, 3B) were also reflected in widefield images (Figure 3C). In WT cells at 14 hpi, multiple capsid assembly sites could be seen in the nucleus and capsids were also associating with the nuclear envelope in most cells irrespective of the viral load (Figure 3C). In *C1GALT1C1* KO cells less and smaller assembly sites could be seen, capsids less frequently associating with nuclear envelope, which slightly improved later in infection (20 hpi) (Figure 3C).

In order to evaluate the contribution of viral glycans to fitness of progeny virus for early interactions with wild type host cells, we added equal numbers of infectious particles, produced in propagation experiments, to WT keratinocyte monolayers following the previously outlined strategy. No defects in binding or entry were found with virions lacking different glycan structures (Figure 3D-H). In fact, virions lacking O-glycan elongation are capable of accelerated binding, despite low viral titers of HSV-1 produced in *C1GALT1C1* KO or *C1GALT1* KO (Figure 3F). This suggests the observed propagation defects are related to host and viral factors influencing the formation of infectious virions and not their efficiency in establishing a new infection.

**Role of site-specific O-glycosylation**

The effect of O-glycosylation on HSV-1 glycoprotein localization, and prior knowledge of O-glycosite modifications compelled us to investigate specific O-glycosites. Eliminating site-specific O-glycosylation may have a more profound effect on protein function than truncation of the O-

glycan structure [5, 35, 36]. Therefore, although O-glycan truncation had no effect on properties of infectious virions, it should not be excluded that individual O-glycosylation sites could play a functional role.

We have previously identified more than 70 O-glycosites on eight out of the 12 HSV-1 surface proteins, including the indispensable fusion machinery comprised of gB, gD, gH, and gL. Based on available structural data and defined molecular mechanisms, we mutated five out of the identified 21 gB O-glycosites and three out of five gD O-glycosites most likely to affect fusion and receptor binding, respectively (Figure 4A, 4F) [15]. We generated Ser/Thr to Ala substitutions alone or in combination to test cell-cell fusion efficiency using a split luciferase reporter assay as a proxy for viral entry (Table S2, Figure S3). The assay quantifies fusion between two cell types, one (effector) lacking HSV-1 entry receptors and transfected with plasmids encoding the conserved fusion machinery, and the other (target) presenting HSV-1 entry receptors (Figure 4B) [37]. Each cell type is also transfected with plasmids encoding half of a split luciferase reporter, which upon cell fusion can form a functional enzyme generating luminescence. In addition, we quantified gB and gD surface expression by CELISA [37].

For gB single site O-glycan mutants, we focused on the domain directly involved in fusion (I), where we identified three sites on antiparallel beta strands (T169, T267, T268), as well as the arm domain (V) comprised of two alpha helices that undergo structural rearrangements upon fusion, where we found one O-glycosite on each (T690 and T703) (Figure 4A) [15, 38, 39]. All mutations except for T268A affected gB cell surface expression; T169A, T267A, and T703A showed moderate reduction, whereas T690A showed increased expression (Figure 4C). T268A exhibited reduced fusion activity, as did T267A, also after accounting for surface expression. Double or triple mutations in domain I severely decreased surface presentation and fusion activity (Figure 4D). Interestingly, T690A exhibited very low fusion activity, whereas T703A was hyperfusogenic, after surface expression adjustment. The domain V double mutant (T690A T703A) had a higher surface expression, and the fusion activity was a sum of the opposite effects of individual mutations, yielding lower activity than the WT protein (Figure 4E).

Though gD does not directly execute fusion, it initiates entry by binding to several different host receptors and reduced gD binding translates to reduced fusion efficiency. For gD, one O-glycan site on the N-terminal tail of the protein (S33 (8)), involved in interaction with both Nectin-1 and

HVEM, and two O-glycan sites on an alpha helix undergoing structural changes upon interaction with HVEM (T255 (230) and S260 (235)), were mutated (Figure 4F) [15, 40-42]. All mutants maintained close to normal levels of cell surface expression of gD and fusion activity, which translated to slightly higher activity after surface expression adjustment (Figure 4G, 4H).

In conclusion, we identified functionally relevant O-glycan acceptor amino acids on gB, directly executing fusion, but no effects were observed for the initial engager gD in the presence of multiple host entry receptors.

**Spread of HSV-1 in mutant cell lines**

Lastly, we investigated the roles of the specific classes of glycans in direct cell-to-cell spread mediated in part by gE/gI via cell contacts of 2D grown keratinocytes, and unrestricted spread in 3D skin culture, facilitated by tissue destruction and release of free virions (Figure 5A).

We first performed plaque assays with 2D grown cells, where dissociation of progeny virions is restricted. Perturbations in core 1 O-glycan biosynthesis resulted in increased plaque size, most notably in *C1GALT1* KO and *ST3GAL1* KO cells (Figure 5B). Upon plaque immunostaining, WT cells and KO cells exhibiting increased plaque size showed strong gE expression on the cell surface (Figure 5C). In cells lacking N-linked glycan maturation (*MGAT1* KO) and those lacking MGAT4B (*MGAT4B* KO; *MGAT5+MGAT4B* KO), resulting in reduced β4-antenna branching, we found a markedly reduced cell-to-cell spread (Figure 5B). *MGAT1* KO cells showed less pronounced and more punctate gE expression, which may be linked to N-glycosylation sites on gE and help explain the limited spread capacity. Surprisingly, accelerated spread was observed in *MGAT4A* KO cells, which also contributes to β4-antenna branching, and a similar tendency was observed for *MGAT5* KO, devoid in β6-linked antenna branching.

To assess viral spread in tissue, we infected fully developed 3D epidermises built with the glycoengineered cells (Figure 5D). Different spread characteristics were observed, when viral spread was not limited to cell-to-cell contacts mediated by gE/gI complex. In wild type HaCaT skin equivalents trans epidermal lesions were observed at 36 hpi (Figure 5E, 5F). To avoid selection bias, we generated ten subsequent tissue sections separated by 30 microns and scanned whole sections, which allowed to visualize and compare the extent of the viral lesions (Figure 5D, 5E,

Figure S4). We identified lesions spanning several sections and measured the cross-section areas corresponding to the central regions of those lesions (Figure 5G). Large lesions were seen in *MGAT1* KO tissues, contrasting the small plaques observed in 2D (Figure 5F, 5G). Most N-glycan branching KO tissues, especially *MGAT4A* KO and *MGAT5+4B* KO, permitted only limited spread in the top layers of the epidermis. *MGAT4B* KO allowed formation of bigger lesions, but the tissue penetrance was limited, which was also the case for tissues with reduced core 1 sialylation (*ST3GAL1* KO) (Figure 5F, 5G). No significant spread defects were noted for tissues with disruptions in GSL and GAG synthesis.

**Discussion**

We utilized a genetically engineered keratinocyte library to systematically investigate the contributions of different classes of glycan structures to multiple stages of HSV-1 life cycle in the natural context of infection. This approach allowed the discovery that each class of glycans modulated select stages of the viral life cycle, and we narrowed down the critical biosynthetic steps mediating these effects. We found chain-specific GAG sulfation, GSL sialylation and antenna-specific N-glycan branching important for attachment, O-glycan core synthesis important for propagation, and complex N-glycans important for cell-to-cell and tissue spread. In addition, reducing the complexity of the O-glycome potentiated attachment, and cell-to-cell spread. Since distinct glycan classes could independently finetune early virus-host interactions, we suggest that HSV-1 through its evolution developed elaborated mechanisms to exploit the host glycosylation machinery.

We obtained the most unequivocal effects on HSV-1 infection upon GAG- and GSL-associated perturbations in the glycocalyx. Most previous studies investigating the roles of GAGs and GSLs are based on isolated systems involving synthetic (glyco)conjugates and isolated or overexpressed viral proteins, often in non-permissive cells. While HSV-1 has been shown to interact with both terminal HS and CS glycan chains in solution or on solid support [27, 31, 32], data on HSV-1 interaction with GAGs attached to their intrinsic core proteins and presented in their native context of the glycocalyx is only beginning to emerge [43]. We here demonstrated that binding of viral particles to human keratinocyte monolayers lacking GAG moieties on proteoglycans on ice

was almost completely inhibited, emphasizing the role of GAGs in very early interactions. Despite of this, HSV-1 propagated well in *B4GALT7* KO cells. This agrees with HSV-1 being able to infect mouse cells almost devoid of GAGs (sog9), especially at higher viral loads [44], and with increased release of virions from cells upon overexpression of heparanase [45]. This underscores the contextualized functions of glycans as modulators of molecular interactions, which only become obligate under specific stress conditions [6]. Our findings complement the well documented role of glycosaminoglycans in herpesvirus biology [26, 27, 31, 46-48]. It is proposed that GAGs allow HSV particles to "surf" on the cell surface until encountering cognate receptors for gD and initiating entry. Lack of such interactions has been demonstrated to prevent free movement of the viral particles on membrane equivalents or the surface of cells, and distinct roles of HS and CS in promoting lateral diffusion or confinement has recently been suggested [43, 47]. By using a genetic approach, we determined that sulfated HS is the major contributor of HSV-1 gC binding to CHO cells, with CS not able to sustain the interaction in the absence of HS. By selective desulfation of purified HS, it has previously been shown that 2-O, 6-O, and N-sulfation, and at least a fragment of 12 monosaccharides is needed for optimal gC-HS interaction [32]. gC was still able to bind de-N-sulfated HS partially [32], confirming that N-sulfation, genetic depletion of which completely abolished gC binding in our study, is also important for creation of sulfate-rich GAG patches by follow-up 2-O and 6-O sulfation.

After attachment, HSV-1 enters keratinocytes either via direct membrane fusion or endocytosis, and both of these routes are thought to be cholesterol-rich lipid raft dependent and involving interactions between viral and cellular proteins [25, 28, 49-51]. Mechanistic insight into the interaction of sphingomyelin and cholesterol with HSV-1 gH leading to membrane fusion is available [52]. In contrast, knowledge on the role of glycosphingolipids, another major component of lipid rafts, in HSV-1 biology is scarce. Here, we show that elongation of host GSLs beyond glucosylceramide is important for efficient viral binding and entry. It is suggested that αVβ3-integrin reroutes nectin 1 to lipid rafts thus promoting cholesterol-mediated entry [53]. It is therefore plausible that altering the composition of lipid rafts by changing the GSL content may interfere with proper nectin 1 trafficking as well as membrane fusion dynamics via gH.

We identified diverse effects on the infectious cycle attributable to select maturation or branching steps of protein-bound N- and O-linked glycans. Investigating the importance of complex N-linked

glycans, we saw significantly smaller plaque size in *MGAT1* KO cells, indicating diminished cell-to-cell spread, while viral titers were only marginally reduced. Both observations are in accordance with previous investigations in a ricin-resistant baby hamster kidney cell line RicR14, deficient in Mgat1 activity [54]. In contrast to the previous studies, we did, however, observe an increase in the ratio of viral DNA to infectious particles, and an altered localization of envelope glycoproteins gB and gD, suggestive of less productive assembly in cells lacking complex N-glycans. Furthermore, we detected lower adsorption of HSV-1 to *MGAT1* KO cells. In another ricin resistant cell line, Ric21, presenting with N-linked glycans of reduced complexity and sialylation, HSV-1 infection also showed smaller plaque size and retarded particle production [55], suggesting the effects we see in *MGAT1* KO cells may be related to lack of sialylation. Accordingly, treatment of HSV-1 viral particles with α2,6 specific neuraminidase has previously been shown to dramatically reduce the infectivity of viral particles [56]. However, we did not observe diminished binding of infectious particles bearing immature N-glycans lacking sialylation despite N-linked glycans being the major acceptors of α2,6-linked sialic acids in keratinocytes.

The use of cell lines defective in N-glycan branching allowed us to differentiate between contribution of β4-linked and β6-linked antennae and compare it to complete loss of N-glycan maturation. While we did not see any importance of β6-linked antennae, generated by MGAT5, we found decreased binding of wild type HSV-1 to and diminished cell-to-cell spread in *MGAT4B* KO cells, which is the main contributor to β4-linked antenna synthesis. Interestingly, MGAT4A, another isoform capable of generating β4-linked antennae, selectively reduced entry to host cells and dramatically increased HSV-1 spread in mutant cell monolayers. MGAT4A and MGAT4B are differentially expressed with MGAT4B being most abundant [57] and differential substrate protein preferences have recently been shown *in vitro* possibly regulated via the C-terminal lectin domain [29, 30]. The distinct effects of the two enzymes are also demonstrated in *MGAT4A* KO mice presenting with hyperglycemia due to selective N-glycan branching of the GLUT2 transporter by MGAT4A, despite the co-expression of MGAT4B in the pancreas [57, 58]. Moreover, glycosyltransferases have been described to form complexes with each other and with nucleotide sugar transporters in the Golgi membrane, and it has been shown that MGAT1 interacts with MGAT4B, but not MGAT5 [59]. It is therefore possible, that such complex formation or lack thereof is affecting secretory pathway dynamics and protein substrate selectivity. This may help

explain the comparable effects on virus-cell binding and cell-cell spread for *MGAT1* KO and *MGAT4B* KO suggesting importance of select N-glycosylation by MGAT4B of specific cellular proteins, and the distinct phenotypes caused by KO of *MGAT4A*.

We previously demonstrated the importance of mucin type O-glycan elongation for HSV-1 propagation and early immune sensing [15, 60]. Here, O-glycan biosynthesis was dissected to include branching and capping steps. We discovered that the decreased viral titers and fitness were associated with complete truncation of O-glycans to $\alpha$-GalNAc by KO of *C1GALT1* or its chaperone *C1GALT1C1*, and not with loss of sialylation of core 1 structures by ST3GAL1 or reduced core 2 branching by GCNT1. In fact, lack of core 2 structures on host cells resulted in accelerated binding and thus entry of WT virus to cells. Since core 2 structures comprise a significant portion of the cellular O-glycome, it is plausible that the reduced complexity on the cell surface would allow better accessibility. Loss of O-glycan elongation affected glycoprotein localization, with lower gD surface presentation, and altered gB localization, possibly influencing their incorporation into viral particles in turn affecting the proportion of particles capable of productive infection. In addition, gB is needed for de-envelopment at the outer nuclear membrane [61], and perturbed localization due to loss of O-glycans could contribute to lower release rate of capsids to the cytosol. In contrast, loss of core 1 elongation or sialylation allowed for accelerated cell-to-cell spread mediated by HSV-1 gE and gI, where competent surface expression of the former protein suggests protein-selective effects of O-glycans for proper localization.

We have previously shown that HSV-1 and other herpesviruses are heavily O-glycosylated [15, 62]. To investigate the function of O-glycans at specific sites we used a cell-based assay probing the function of viral entry machinery consisting of gB, gD, gH and gL. We focused on specific O-glycan acceptor amino acids on gB and gD. In the fusion effector gB we selected three O-glycosites (T169, T267, T268) decorating the central region of the beta sheet terminating in fusion loops (domain I). In addition, we examined two O-glycosites (T690, T703) present on the internal alpha helices important for reinforcing trimer interactions and undergoing extensive reorientation upon fusion (domain V) [15, 38, 39]. We hypothesized that the glycans, due to their critical positioning, could modulate the conformational stability and rearrangements of their respective domains. When eliminating specific O-glycan acceptor sites within domains directly or indirectly involved in fusion (I and V, respectively) we saw a clear effect on gB function and cell surface expression. Some

mutations diminished fusion (T267A, T268A, T690A) and others accelerated it (T703A). One of the positions (T690) has previously been identified to reduce gB function by linker insertion mutagenesis, where reduced cell surface expression was also seen [63]. This is in contrast to our observed increased surface presentation of T690A mutant. Hyperfusogenic mutations in the gB ectodomain are rare, while such mutations are often found in the cytoplasmic tail [64, 65]. Hyperfusogenic mutations have been shown to affect the stability of the trimer in the pre-fusion conformation and the energy barrier threshold for executing fusion [66]. It will be important to validate the effect is truly glycan dependent and not influenced by the change in amino acid itself, and to define O-glycan occupancy on HSV-1 virions. Nevertheless, the work identifies new hotspots in gB structure that could be targeted for disrupting protein function. In contrast, infectious virions bearing truncated O-glycans did not exhibit any defects in binding or entry; in fact, we observed accelerated binding, suggesting that even very short O-glycans are sufficient for maintaining functions of properly localized proteins. In contrast, eliminating site-specific glycosylation on gD did not diminish cell-cell fusion. Since HEK293 cells express multiple receptors for gD, alternative receptor usage likely would rescue inefficient binding to one of the receptors. It would therefore be useful to explore cell lines expressing one entry receptor at a time to evaluate the effects of O-glycosite mutations on isolated interactions.

In further attempts to examine contextualized functions of glycans in a biologically relevant system, we utilized the ability of keratinocytes to form stratified epithelia to investigate viral spread in glycoengineered tissue. Strikingly, we saw very different effects of glycans in 3D tissue spread compared to overlaid monolayers. This suggests the effects we see in 2D are directly related to importance of glycans on gE/gI complex or their receptors, whereas 3D spread involves both cell-to-cell and virus-to-cell transmission, and is also influenced by changes in tissue architecture induced by glycogene KOs.

In addition to uncovering functions of distinct classes and subtypes of cellular glycans, we also shed light on the requirement of viral glycans for proper function. HSV-1 particles are shown to contain both N-linked and O-linked glycans, and it is expected that glycosphingolipids are part of the cell membrane-derived viral envelope [15-18]. It is not known whether proteoglycans decorated with GAGs can be incorporated into HSV-1 particles, but they were not detected in a proteomic study looking at cellular proteins incorporated into HSV-1 membranes [67]. While we

identified ample functions of the host cellular glycans for HSV-1 biology, we found limited effects of glycome perturbations on properties of progeny virions able to establish infection.

By using a glycoengineered keratinocyte library, we show that different classes and subtypes of glycans play very selective roles in specific stages in HSV-1 life cycle. We conclude that through evolution HSV-1 developed an elaborate network of interactions with different cellular glycans to allow for efficient entry and propagation, which could be explored for glycan-targeted intervention strategies. Individual findings of this exploratory study shall be the scope of future investigations.

## Materials and methods

### Cells and viruses

The HaCaT human keratinocyte WT and genetically engineered cell lines were grown in DMEM supplemented with 10 % FBS (HyClone) and 4 mM L-glutamine. CHOZN GS -/- (glutamine synthetase KO; WT CHO (Sigma)) and genetically engineered cell lines [33] were grown in EX-CELL® CD CHO Fusion serum free media mixed 1:1 with BalanCD CHO growth media and supplemented with 2 % L-glutamine in 50 mL TPP TubeSpin® Bioreactors. DMEM mixed 1:1 with Ham's F12 nutrient mix and supplemented with 10 % FBS (Gibco) and 4 mM L-glutamine was used for adherent CHO cell culture. HEK293 Ac2 cells were grown in DMEM supplemented with 10 % FBS (Gibco) and 4 mM L-glutamine. The wild-type HSV-1 virus Syn17+ [68] was used throughout the study, and the virus titers were determined by plaque titration on Green monkey kidney (GMK, obtained from the Swedish Institute for Infectious Disease Control, Stockholm) cells as previously described [69]. HSV-1 Syn17+ virus was cultivated in HaCaT wild type keratinocytes or GMK cells depending on downstream application and the titers were determined as mentioned above. K26GFP HSV-1 [70] was a kind gift from Prashant Desai (The Johns Hopkins University), and cultivated as mentioned above.

### ZFN and CRISPR/Cas9 gene targeting

HaCaT KO library was generated using ZFN nuclease and CRISPR/Cas9 technology by targeting particular glycogene exons by validated gRNAs [71] or gRNAs predicted by GPP [72]. gRNAs were cloned [73] using oligos (TAGC, Denmark) into lentiCRISPR-v2-Puro plasmid backbone (Addgene

#52961) or lentiCRISPR-v2-Blast with a blasticidin resistance gene replacing the puromycin resistance gene (Brakebusch laboratory, BRIC, UCPH, DK). Directional cloning and insertion of the gRNA duplex using BsmBI and T4 ligase into the LentiCRISPR-v2 plasmid backbone was done as described earlier [74]. All plasmids were propagated in One Shot™ Stbl3™ Chemically Competent *E. coli* cells (Thermo Fisher). Endonuclease free plasmid preparations were made using Midi Prep kit (Thermo Fisher). For lentivirus production HEK293T cells were seeded at $1x10^5$ cells/well density in a 6-well plate and grown for 72 h until 80-90% confluence. For transfection, 200 µL OPTI-MEM (Gibco), 8 µL of 1 mg/mL PEI (Sigma), 0.8 µg LentiCRISPR-V2-gRNA plasmid, 0.6 µg pCMV-VSV-G plasmid (Addgene #8454), and 0.6 µg psPAX2 plasmid (Addgene #12260) were mixed and incubated for 10 min at RT before added to the adherent HEK293T cells. After 24 h the transfection media was replaced with HaCaT media for harvesting virus for transduction. Medium containing viral particles was collected 48/72 h post-transfection, i.e. when virus had accumulated for 24 h after medium change, filtered (0.45 µm pore size). Filtered virus-containing medium was mixed 1:1 with fresh HaCaT media and 1:1000 polybrene (Sigma), and used to transduce HaCaT cells overnight [75]. Selection of KO cell lines started 48-96 hours after transduction, with either 5 µg/ml blasticidin S (Gibco) or 1 µg/ml puromycin (Gibco) including biweekly cell passaging. Single clones were obtained by serial dilution in 96 well plates and KO clones were identified by IDAA using ABI PRISM™ 3010 Genetic Analyzer (Thermo Fisher) and Sanger sequencing (GATC, Germany). Two to five clones were selected for each gene with out of frame indel formation. IDAA results were analyzed using Peak Scanner Software V1.0 (Thermo Fisher) [76].

**MS-based glycan profiles**

For O-GalNAc profiles, the Cellular O-Glycome Reporter/Amplification (CORA) method was used as described in [77]. In brief, HaCaT cells were seeded in 6-well plates, and when the cells reached 70 % confluence, the medium was supplemented with 100 µM Bn-α-GalNAc or DMSO for untreated controls. Media was harvested after 48 h and passed through a 10-kDa Omega membrane (Pall Corporation) followed by purification with a Sep-Pak 3-cc C18 cartridge (Waters). Samples were then concentrated by SpeedVac to remove organic solvent and lyophilized. For profiling of N-linked glycans, HaCaT cell pellets were dissolved in 0.1 % Rapigest (Waters) and incubated on ice and vortexed every 5 minutes. Samples were then centrifuged at 10000 g for 10 min and the supernatant was collected and reduced with 5 mM DTT (Sigma) for 1 h at 60 °C followed by

alkylation with iodoacetamide (Sigma) for 30 minutes at RT while kept dark. Samples were digested with 5 µg trypsin (Roche Diagnostics) overnight at 37 °C and peptides were purified with a Sep-Pak 1-cc C18 cartridge (Waters). Organic solvent was removed by SpeedVac and pH was adjusted to 7-8 with 50 mM ammonium bicarbonate, followed by overnight digestion with 3 U PNGase F (Roche diagnostics) at 37 °C. Released N-glycans were cleaned up on a Sep-Pak 1-cc C18 cartridge and lyophilized. For N-glycan profiles, dried samples were permethylated as described previously [78] and analysed by positive reflector mode MALDI-TOF (AutoFlex Speed, Bruker Daltonics) with data acquisition in the 1000-5000 m/z range. For O-glycans the data acquisition was in the 500-3500 m/z range.

**Organotypic culture**

Organotypic cultures were prepared as described by Dabelsteen et al. [36, 79]. Briefly, human fibroblasts were suspended in acid-extracted type I collagen (4 mg/mL) and allowed to gel over a 1-mL layer of acellular collagen in six-well culture inserts with 3-µm-pore polycarbonate filters (BD Biosciences NJ, USA). Gels were allowed to contract for 4–5 days before seeding with $3x10^5$ HaCaT keratinocytes in serum and mitogen-supplemented DMEM/F12 raft medium. Inserts were raised to the air-liquid interface 4 days after cell seeding, and the media changed every second day for an additional 10 days. Infection of organotypic cultures was performed as previously described with minor modifications [80]. Briefly, media was removed on day 9 after insert raising, and 3000 PFU of HSV-1 Syn 17+ applied in 500 µL of RAFT media to the to the top of the cultures, let drip through in 15 min, and reapplied 3 more times during 1 hour. RAFT media was then added to cover the bottom of the organotypic cultures and incubated for 36 more hours until harvesting.

**Propagation assay**

HaCaT cell monolayers in 6 wells in triplicates were washed with PBS and infected with MOI 10 of HSV-1 Syn 17+. The virions in 1 mL of DMEM P/S were adsorbed at 37 °C with periodical rocking of the plates for 1 hour, inoculum removed and cells washed with PBS, followed by addition of 2 mL/well of DMEM supplemented with 10 % FCS and P/S. Virus was harvested at 17 hours post infection. Media was spun at 3000 rpm for 10 min at 4 °C, supernatant aliquoted and stored at -80 °C. Cell monolayers were washed with PBS, dissociated with TrypLE reagent, spun at 100 x g for 5

min, washed with PBS, aliquoted and spun at 400 x g for 5 min, supernatant removed and cells stored at -80 °C.

**Plaque assay**

Titers of virus produced in HaCaT keratinocytes were determined on Green monkey kidney (GMK) cells. Cell monolayers were infected with serial dilutions of virus and allowed to attach. After 1 h the inoculum was removed and the cells overlaid with medium containing 1 % methylcellulose (Sigma-Aldrich), 2.5% FCS, 100 unit/mL penicillin and 100 µg/mL streptomycin (in HBSS (Sigma-Aldrich) + DMEM (Gibco, Life Technologies) at a ratio of 1:1). After 48 h incubation, the overlay medium was removed, the cells fixed with 1 % crystal violet (in 70 % EtOH/37 % formaldehyde/acetic acid 20:2:1 v/v/v), washed 4x times with water and allowed to dry. The resulting plaques were inspected and counted using a light microscope (Olympus IMT-2). Plaque size was measured using AxioVision software.

**DNA extraction and qPCR**

DNA was extracted using the NucleoSpin® Tissue Kit (Macherey-Nagel) according to manufacturer's instructions. Media was diluted 200x before extraction and 100 µL used for extraction. DNA was eluted in 100 µL volume. For assessing the DNA copy number of HSV-1, a 118-nucleotide segment of the gB-1 region was amplified with primers described in [81]. The qPCR reaction volume was set to 20 µL and contained 4 µL HOT FIREPol®Probe qPCR Mix Plus (ROX) (Solis Biodyne), primers and probe (forward primer at 0.5 µM, reverse primer at 0.5 µM and probe at 0.3 µM final concentrations), and 1 µl of DNA. Amplification of the target sequence was performed using the StepOne Plus system (Thermo Scientific). The reaction conditions were set to 10 min at 95 °C followed by 45 PCR cycles of two-step amplification (15 sec at 95 °C and 60 sec at 60 °C). HSV-1 Forward 5'-GCAGTTTACGTACAACCACATACAGC-3'; HSV-1 Reverse 5'-AGCTTGCGGGCCTCGTT-3'; HSV-1 Probe FAM-5'-CGGCCCAACATATCGTTGACATGGC-3'-MGBNFQ (Thermo Fisher Scientific). The efficiency of each round of PCR was determined using 10-fold dilutions of Topo TA plasmids (Invitrogen AB, Stockholm, Sweden) with insert of respective amplicon created according to the manufacturer's instructions.

**Binding and entry assays**

Binding and entry assays were performed as previously described [82]. HaCaT cell monolayers were prechilled on ice for 30 min. For binding assay, 200 PFU of HSV-1 Syn 17+ WT or glycoengineered HSV-1 in 1 mL DMEM supplemented with 2.5 % FCS, 100 unit/mL penicillin and 100 µg/mL streptomycin (P/S) was added on cell monolayers on ice in triplicates, and incubated for 20 or 120 min. After the indicated time points, cells were washed twice with ice-cold PBS and overlain with 2 % methylcellulose in HBSS, mixed 1:1 (v/v) with DMEM supplemented with 5 % FCS, 200 unit/mL penicillin and 200 µg/mL streptomycin. Overlain monolayers were incubated at 37 °C and 5 % $CO_2$ for 48 h, overlay media removed, cells fixed and stained with 1 % crystal violet in 70 % EtOH/37 % formaldehyde/acetic acid (20:2:1 v/v/v), washed 4 times with MQ $H_2O$, dried, and plaques counted using a light microscope (Olympus IMT-2). For entry assay, after 120 min on ice, the inoculum was removed, washed with room temperature DMEM, P/S, and 1 mL of room temperature DMEM supplemented with 2.5 % FCS and P/S was added, followed by a 5 min incubation at 37 °C. The plates were then returned on ice, media removed and non-entered particles inactivated with ice-cold citrate buffer (40 mM citric acid, 10 mM KCl, 135 mM NaCl pH 3) for 2 min, then washed twice with ice-cold PBS and overlain with media as described above. A 0 min time point without shift to 37 °C was used as control.

**Antibodies and probes**

Mouse anti-gB (HSV-1B11D8), anti-gC (B1C1B4), anti-gD (C4D5G2) and anti-gE (B1E6A5) mAbs, as well as recombinant gC probe were produced at the University of Gothenburg [83]. Rabbit anti-E-cadherin mAb (24E10) was purchased from Cell Signaling Technology and goat anti-HSV-1-FITC pAb (GTX40437) from Genetex. Goat anti-mouse IgG AF647 $F(ab)_2$, goat anti-mouse IgG AF594 (H+L), goat anti-mouse IgG AF488 (H+L), and donkey anti-rabbit IgG AF546 (H+L) were all from Thermo Fisher Scientific. Rabbit anti-mouse Igs HRP was from DAKO.

**Immunofluorescence**

HaCaT cells grown on glass cover slips in 24-wells were infected with MOI 10 of HSV-1 K26-GFP. 14 hours post-infection the cells were washed 2x with Hanks Balanced Salt solution (HBSS, Sigma-Aldrich Cat. Nr. H8264) and fixed with 4 % PFA in PBS (Ampliqon Cat. Nr. AMPQ44154.1000) for 15 min at RT followed by 2x more washes. The cells were permeabilized with 0.3 % Triton X-100 in HBSS for 3 min followed by 2x washes with HBSS and blocked with 2.5 % BSA in HBSS, 0.03 %

sodium azide at RT for 45 min. Cover slips were incubated with primary antibodies diluted in blocking buffer at 4 °C over night followed by 3x washes with HBSS and incubation with secondary antibodies at RT for 45 min. The cover slips were rinsed with HBSS and incubated with 0.1 µg/mL DAPI solution in HBSS for 5 min followed by 3x washes and mounting with Prolong Gold antifade-reagent (Thermo Fisher Scientific Cat. Nr. P36930). For stainings of non-infected HaCaT cells with gC probe, fixed and permeabilized cells on cover slips were treated with either chondroitinase ABC (0.25 mU), heparinases 1, 2 and 3 (0.25 mU of each), or left untreated for 1 hour at 37 °C followed by incubation with 2 µg/mL gC probe diluted in 2.5 % BSA in PBS, 0.03 % sodium azide for 1 hour at RT, 3x washes with PBS and staining with mouse anti-gC mAb as described above, though using PBS-based blocking buffer and washes. For plaque stainings HaCaT cells grown on large cover slips in 6 wells were infected with 200 PFU of HSV-1 K26-GFP and overlaid with DMEM, 2.5 % FCS, 1 % methylcellulose, 100 unit/mL penicillin, 100 µg/mL streptomycin for 48 hours. Therafter the overlay media was removed, cover slips washed 3x with PBS and fixed in 4 % PFA in PBS for 25 min followed by 3x washes and blocking in 2.5 % BSA in PBS, 0.03 % sodium azide at 4 °C over night and staining procedure as described above, though with primary Ab incubation for 2 hours at RT and dilutions in 2.5 % BSA in PBS, 0.03 % sodium azide. Images were documented using Zeiss LSM710 confocal microscope. FFPE organotypic tissue sections were deparaffinized and microwave treated for antigen retrieval (Tris-HCl buffer pH 9). The sections were then permeabilized with 0.3 % Triton X-100 in PBS, washed 3x and incubated with goat anti-HSV-1-FITC pAb (GeneTex, 1:50 in 2.5 % BSA in PBS, 0.03 % $NaN_3$) for 2 h at room temperature, followed by 3 washes with PBS and mounting with ProLong™ Gold antifade reagent with DAPI (Thermo Fisher Scientific). Entire sections were imaged using Zeiss AxioScan microscope. Images were assembled using Adobe Photoshop 2021, Adobe Illustrator 2021, or Zeiss ZEN Lite software.

**Flow cytometry**

Cell surface binding studies were carried out by flow cytometry analysis. First, cells were counted and 1 x $10^5$ cells/well were distributed into U-bottom 96-well plate (TermoFisher Scientific™ Nunclon™ Delta surface). Cell viability was evaluated by trypan blue stain, applying a viability requirement of > 95 % for cells to be included for analysis. Next, cells were washed once in ice-cold PBS, centrifuged at 500 x g for 3 min at 4 °C. Cells were then incubated with recombinant gC protein (0.5 µg/mL) diluted in ice-cold PBS with 2 % FBS, for 45 min at 4°C. Following, cells were

washed twice in ice-cold PBS with 2 % FBS before incubation with mouse anti-gC mAb B1C1B4 (2 µg/mL) diluted in PBS with 2 % FBS for 45 min at 4 °C. After incubation, cells were washed twice in ice-cold PBS with 2 % FBS and incubated with goat anti-mouse IgG (H+L) AF488 (1:1000) diluted in PBS with 2 % FBS for 45 min at 4 °C in the dark. Lastly, cells were washed twice with PBS with 2 % FBS, and suspended in 100 µL PBS with 2 % FBS for analysis. Fluorescence intensity was measured on the SONY Spectral Cell Analyzer (SONY SA3800). A total minimum of 10 000 events were recorded for analysis. Cell debris and doublets were excluded based on FSC-A/FSC-H plot to ensure analysis based on singlets. Data is presented as the geometric mean of samples incubated with gC probe, after substraction of the geometric mean of background fluorescence, samples incubated with primary and secondary antibody only, and normalized to WT. All data analysis was done using FlowJo V. 10.0.7.

**Plasmids and cloning**

Plasmids encoding full length HSV-1 gB (pMTS-1-gB), gD (pcDNA3.1(-)-gD), gH (pMTS-1-gH), and gL pMTS-1-gL) was a kind gift from Gabriella Campadelli-Fiume (University of Bologna). Plasmids encoding split luciferase (DSP1-7, DSP8-11) were kindly provided by Zene Matsuda (University of Tokyo). Single and multiple amino acid mutations in gB and gD were introduced using custom primers (Table S2) and the QuikChange Lightning Multi Site-Directed Mutagenesis Kit according to manufacturer's instructions. Briefly, mutagenic primers were annealed and extended during 30 thermal cycles (2 min 95 °C; 30 x (20 sec 95 °C, 30 sec 55 °C, 30 sec/kb 65 °C); 10 min 65 °C), followed by template digestion with DpnI, and transformation into XL10-Gold Ultracompetent Cells. The transformation reactions were plated on LB-carbenicillin agar plates and colonies screened by PCR using Herculase II Fusion Pfu DNA Polymerase (Agilent) followed by Sanger sequencing. Colonies of interest were re-streaked, grown up in LB-carbenicillin media and Mini Preps prepared using Zyppy Plasmid Miniprep Kit (Zymo Research) followed by Sanger sequencing. Subsequently, plasmid Midi Preps were prepared using NucleoBond Xtra Midi Endotoxin-free Kit (Macherey-Nagel).

**Split-luciferase assay**

The assay was performed as previously described [37] with several modifications. CHO K1 cells (effector) grown in Greiner CELLSTAR® white polystyrene 96 well plates were transfected with 375

ng/well of gB, as well as 125 ng of each gD, gH, gL, and DSP1-7 plasmids using Lipofectamine 3000 (Thermo Scientific) according to manufacturer's instructions in triplicates. Plasmids encoding wild type or mutated gB or gD were used. An additional clear polystyrene plate with transfected cells was prepared for CELISA measurements. HEK293 cells (target) grown in 6 well plates were transfected with 1 μg/well of DSP8-11 plasmid. For split-luciferase assay, 23 hours post-transfection, the media of CHO K1 cells was replaced with fusion media (DMEM (no phenol red), 5 % FCS, 50 mM HEPES), supplemented with EnduRen substrate (Promega, 1:1000) and incubated at 37 °C for 1 hour. HEK293 cells were detached using 0.02 % EDTA in PBS, resuspended in fusion media and added to effector cells. Luminescence was measured every 2 min for 240 min at 37 °C using EnSpire plate reader (Perkin-Elmer).

**CELISA**

Cell surface ELISA was performed as previously described [37] with several modifications. 96w plates with transfected cells were washed 3x with PBS supplemented with divalent cations (0.9 mM $CaCl_2$, 0.5 mM $MgCl_2$ ($PBS^{2+}$)) 20 hours post-transfection and fixed with 4 % PFA in PBS for 10 min followed by 3x washes and blocking in 3 % BSA in $PBS^{2+}$ for 30 min. The cells were then incubated with mouse anti-gB (1:20) or anti-gD (1:100) mAbs in blocking buffer for 1 hour at room temperature, followed by 5x washes and incubation with rabbit anti-mouse Igs HRP (1:500) for 45 min and 6x washes. Plates were developed using TMB + substrate chromogen (Thermo Scientific) and stopped with 0.5 M $H_2SO_4$. The absorbance at 450 nm was quantified using BioTek Synergy LX plate reader.

**Acknowledgements**

We thank Karin Uch Hansen for technical assistance. We acknowledge the Core Facility for Integrated Microscopy, Faculty of Health and Medical Sciences, University of Copenhagen. We kindly thank Prashant Desai, Zene Matsuda, and Gabriella Campadelli-Fiume for sharing virus strains and plasmids. We also thank Gary Cohen and Doina Atanasiu for their valuable guidance. This work was supported by Lundbeck Foundation (R219-2016-545), Danish National Research Foundation (DNRF107) and European Comission (GlycoSkin H2020-ERC).

**Declaration of interests**

HHW owns stocks and is a consultant for and co-founder of EbuMab, ApS, Hemab, ApS, and GO-Therapeutics, Inc. All other authors declare no conflicts of interest.

**References**


1. Bagdonaite I, Wandall HH (2018) Global aspects of viral glycosylation. *Glycobiology* **28**: 443-467
2. Varki A (2017) Biological roles of glycans. *Glycobiology* **27**: 3-49
3. Schjoldager KT, Narimatsu Y, Joshi HJ, Clausen H (2020) Global view of human protein glycosylation pathways and functions. *Nat Rev Mol Cell Biol* **21**: 729-749
4. Wandall HH, Nielsen MAI, King-Smith S, de Haan N, Bagdonaite I (2021) Global functions of O-glycosylation: promises and challenges in O-glycobiology. *Febs j*
5. Bagdonaite I, Pallesen EM, Ye Z, Vakhrushev SY, Marinova IN, Nielsen MI, Kramer SH, Pedersen SF, Joshi HJ, Bennett EP*, et al.* (2020) O-glycan initiation directs distinct biological pathways and controls epithelial differentiation. *EMBO Rep* **21**: e48885
6. Dabelsteen S, Pallesen EMH, Marinova IN, Nielsen MI, Adamopoulou M, Rømer TB, Levann A, Andersen MM, Ye Z, Thein D*, et al.* (2020) Essential Functions of Glycans in Human Epithelia Dissected by a CRISPR-Cas9-Engineered Human Organotypic Skin Model. *Dev Cell*
7. Büll C, Nason R, Sun L, Van Coillie J, Madriz Sørensen D, Moons SJ, Yang Z, Arbitman S, Fernandes SM, Furukawa S*, et al.* (2021) Probing the binding specificities of human Siglecs by cell-based glycan arrays. *Proc Natl Acad Sci U S A* **118**
8. Narimatsu Y, Joshi HJ, Nason R, Van Coillie J, Karlsson R, Sun L, Ye Z, Chen YH, Schjoldager KT, Steentoft C*, et al.* (2019) An Atlas of Human Glycosylation Pathways Enables Display of the Human Glycome by Gene Engineered Cells. *Mol Cell* **75**: 394-407.e5
9. James C, Harfouche M, Welton NJ, Turner KM, Abu-Raddad LJ, Gottlieb SL, Looker KJ (2020) Herpes simplex virus: global infection prevalence and incidence estimates, 2016. *Bull World Health Organ* **98**: 315-329
10. Itzhaki RF (2021) Overwhelming Evidence for a Major Role for Herpes Simplex Virus Type 1 (HSV1) in Alzheimer's Disease (AD); Underwhelming Evidence against. *Vaccines* **9**
11. Bradshaw MJ, Venkatesan A (2016) Herpes Simplex Virus-1 Encephalitis in Adults: Pathophysiology, Diagnosis, and Management. *Neurotherapeutics* **13**: 493-508
12. Tan IL, McArthur JC, Venkatesan A, Nath A (2012) Atypical manifestations and poor outcome of herpes simplex encephalitis in the immunocompromised. *Neurology* **79**: 2125-32
13. Eisenberg RJ, Atanasiu D, Cairns TM, Gallagher JR, Krummenacher C, Cohen GH (2012) Herpes virus fusion and entry: a story with many characters. *Viruses* **4**: 800-32
14. Johnson DC, Baines JD (2011) Herpesviruses remodel host membranes for virus egress. *Nat Rev Microbiol* **9**: 382-94
15. Bagdonaite I, Norden R, Joshi HJ, Dabelsteen S, Nystrom K, Vakhrushev SY, Olofsson S, Wandall HH (2015) A strategy for O-glycoproteomics of enveloped viruses--the O-glycoproteome of herpes simplex virus type 1. *PLoS pathogens* **11**: e1004784

16. Wenske EA, Bratton MW, Courtney RJ (1982) Endo-beta-N-acetylglucosaminidase H sensitivity of precursors to herpes simplex virus type 1 glycoproteins gB and gC. *Journal of virology* **44**: 241-8
17. Serafini-Cessi F, Dall'Olio F, Pereira L, Campadelli-Fiume G (1984) Processing of N-linked oligosaccharides from precursor- to mature-form herpes simplex virus type 1 glycoprotein gC. *Journal of virology* **51**: 838-44
18. Norden R, Halim A, Nystrom K, Bennett EP, Mandel U, Olofsson S, Nilsson J, Larson G (2015) O-linked glycosylation of the mucin domain of the herpes simplex virus type 1-specific glycoprotein gC-1 is temporally regulated in a seed-and-spread manner. *The Journal of biological chemistry* **290**: 5078-91
19. Cohen GH, Long D, Matthews JT, May M, Eisenberg R (1983) Glycopeptides of the type-common glycoprotein gD of herpes simplex virus types 1 and 2. *Journal of virology* **46**: 679-89
20. Peng T, Ponce de Leon M, Novotny MJ, Jiang H, Lambris JD, Dubin G, Spear PG, Cohen GH, Eisenberg RJ (1998) Structural and antigenic analysis of a truncated form of the herpes simplex virus glycoprotein gH-gL complex. *Journal of virology* **72**: 6092-103
21. Geraghty RJ, Krummenacher C, Cohen GH, Eisenberg RJ, Spear PG (1998) Entry of alphaherpesviruses mediated by poliovirus receptor-related protein 1 and poliovirus receptor. *Science* **280**: 1618-20
22. Montgomery RI, Warner MS, Lum BJ, Spear PG (1996) Herpes simplex virus-1 entry into cells mediated by a novel member of the TNF/NGF receptor family. *Cell* **87**: 427-36
23. Satoh T, Arii J, Suenaga T, Wang J, Kogure A, Uehori J, Arase N, Shiratori I, Tanaka S, Kawaguchi Y*, et al.* (2008) PILRalpha is a herpes simplex virus-1 entry coreceptor that associates with glycoprotein B. *Cell* **132**: 935-44
24. Shukla D, Liu J, Blaiklock P, Shworak NW, Bai X, Esko JD, Cohen GH, Eisenberg RJ, Rosenberg RD, Spear PG (1999) A novel role for 3-O-sulfated heparan sulfate in herpes simplex virus 1 entry. *Cell* **99**: 13-22
25. Gianni T, Salvioli S, Chesnokova LS, Hutt-Fletcher LM, Campadelli-Fiume G (2013) alphavbeta6- and alphavbeta8-integrins serve as interchangeable receptors for HSV gH/gL to promote endocytosis and activation of membrane fusion. *PLoS Pathog* **9**: e1003806
26. Shieh MT, WuDunn D, Montgomery RI, Esko JD, Spear PG (1992) Cell surface receptors for herpes simplex virus are heparan sulfate proteoglycans. *J Cell Biol* **116**: 1273-81
27. Peerboom N, Block S, Altgarde N, Wahlsten O, Moller S, Schnabelrauch M, Trybala E, Bergstrom T, Bally M (2017) Binding Kinetics and Lateral Mobility of HSV-1 on End-Grafted Sulfated Glycosaminoglycans. *Biophys J*
28. Sayers CL, Elliott G (2016) HSV1 Enters Human Keratinocytes by a Nectin-1-Dependent, Rapid Plasma Membrane Fusion Pathway that Functions at Low Temperature. *J Virol*
29. Nagae M, Hirata T, Tateno H, Mishra SK, Manabe N, Osada N, Tokoro Y, Yamaguchi Y, Doerksen RJ, Shimizu T*, et al.* (2022) Discovery of a lectin domain that regulates enzyme activity in mouse N-acetylglucosaminyltransferase-IVa (MGAT4A). *Commun Biol* **5**: 695
30. Osada N, Nagae M, Nakano M, Hirata T, Kizuka Y (2022) Examination of differential glycoprotein preferences of N-acetylglucosaminyltransferase-IV isozymes a and b. *J Biol Chem*: 102400
31. Altgarde N, Eriksson C, Peerboom N, Phan-Xuan T, Moeller S, Schnabelrauch M, Svedhem S, Trybala E, Bergstrom T, Bally M (2015) Mucin-like region of herpes simplex virus type 1

attachment protein gC modulates the virus-glycosaminoglycan interaction. *The Journal of biological chemistry*
32. Feyzi E, Trybala E, Bergström T, Lindahl U, Spillmann D (1997) Structural requirement of heparan sulfate for interaction with herpes simplex virus type 1 virions and isolated glycoprotein C. *J Biol Chem* **272**: 24850-7
33. Chen YH, Narimatsu Y, Clausen TM, Gomes C, Karlsson R, Steentoft C, Spliid CB, Gustavsson T, Salanti A, Persson A*, et al.* (2018) The GAGOme: a cell-based library of displayed glycosaminoglycans. *Nat Methods* **15**: 881-888
34. Wisner TW, Johnson DC (2004) Redistribution of cellular and herpes simplex virus proteins from the trans-golgi network to cell junctions without enveloped capsids. *J Virol* **78**: 11519-35
35. Bagdonaite I, Pallesen EMH, Nielsen MI, Bennett EP, Wandall HH (2021) Mucin-Type O-GalNAc Glycosylation in Health and Disease. *Adv Exp Med Biol* **1325**: 25-60
36. Radhakrishnan P, Dabelsteen S, Madsen FB, Francavilla C, Kopp KL, Steentoft C, Vakhrushev SY, Olsen JV, Hansen L, Bennett EP*, et al.* (2014) Immature truncated O-glycophenotype of cancer directly induces oncogenic features. *Proceedings of the National Academy of Sciences of the United States of America* **111**: E4066-75
37. Saw WT, Matsuda Z, Eisenberg RJ, Cohen GH, Atanasiu D (2015) Using a split luciferase assay (SLA) to measure the kinetics of cell-cell fusion mediated by herpes simplex virus glycoproteins. *Methods* **90**: 68-75
38. Heldwein EE, Lou H, Bender FC, Cohen GH, Eisenberg RJ, Harrison SC (2006) Crystal structure of glycoprotein B from herpes simplex virus 1. *Science* **313**: 217-20
39. Vollmer B, Pražák V, Vasishtan D, Jefferys EE, Hernandez-Duran A, Vallbracht M, Klupp BG, Mettenleiter TC, Backovic M, Rey FA*, et al.* (2020) The prefusion structure of herpes simplex virus glycoprotein B. *Sci Adv* **6**
40. Carfí A, Willis SH, Whitbeck JC, Krummenacher C, Cohen GH, Eisenberg RJ, Wiley DC (2001) Herpes simplex virus glycoprotein D bound to the human receptor HveA. *Mol Cell* **8**: 169-79
41. Di Giovine P, Settembre EC, Bhargava AK, Luftig MA, Lou H, Cohen GH, Eisenberg RJ, Krummenacher C, Carfi A (2011) Structure of herpes simplex virus glycoprotein D bound to the human receptor nectin-1. *PLoS Pathog* **7**: e1002277
42. Krummenacher C, Supekar VM, Whitbeck JC, Lazear E, Connolly SA, Eisenberg RJ, Cohen GH, Wiley DC, Carfí A (2005) Structure of unliganded HSV gD reveals a mechanism for receptor-mediated activation of virus entry. *Embo j* **24**: 4144-53
43. Abidine Y, Liu L, Wallén O, Trybala E, Olofsson S, Bergström T, Bally M (2022) Cellular Chondroitin Sulfate and the Mucin-like Domain of Viral Glycoprotein C Promote Diffusion of Herpes Simplex Virus 1 While Heparan Sulfate Restricts Mobility. *Viruses* **14**
44. Banfield BW, Leduc Y, Esford L, Schubert K, Tufaro F (1995) Sequential isolation of proteoglycan synthesis mutants by using herpes simplex virus as a selective agent: evidence for a proteoglycan-independent virus entry pathway. *J Virol* **69**: 3290-8
45. Hadigal SR, Agelidis AM, Karasneh GA, Antoine TE, Yakoub AM, Ramani VC, Djalilian AR, Sanderson RD, Shukla D (2015) Heparanase is a host enzyme required for herpes simplex virus-1 release from cells. *Nat Commun* **6**: 6985
46. Delguste M, Peerboom N, Le Brun G, Trybala E, Olofsson S, Bergstrom T, Alsteens D, Bally M (2019) Regulatory Mechanisms of the Mucin-Like Region on Herpes Simplex Virus during Cellular Attachment. *ACS Chem Biol*

47. Delguste M, Zeippen C, Machiels B, Mast J, Gillet L, Alsteens D (2018) Multivalent binding of herpesvirus to living cells is tightly regulated during infection. *Science advances* **4**: eaat1273
48. Mårdberg K, Trybala E, Tufaro F, Bergström T (2002) Herpes simplex virus type 1 glycoprotein C is necessary for efficient infection of chondroitin sulfate-expressing gro2C cells. *J Gen Virol* **83**: 291-300
49. Gianni T, Gatta V, Campadelli-Fiume G (2010) {alpha}V{beta}3-integrin routes herpes simplex virus to an entry pathway dependent on cholesterol-rich lipid rafts and dynamin2. *Proc Natl Acad Sci U S A* **107**: 22260-5
50. Nicola AV, Hou J, Major EO, Straus SE (2005) Herpes simplex virus type 1 enters human epidermal keratinocytes, but not neurons, via a pH-dependent endocytic pathway. *J Virol* **79**: 7609-16
51. Rahn E, Petermann P, Hsu MJ, Rixon FJ, Knebel-Mörsdorf D (2011) Entry pathways of herpes simplex virus type 1 into human keratinocytes are dynamin- and cholesterol-dependent. *PLoS One* **6**: e25464
52. Vitiello G, Falanga A, Petruk AA, Merlino A, Fragneto G, Paduano L, Galdiero S, D'Errico G (2015) Fusion of raft-like lipid bilayers operated by a membranotropic domain of the HSV-type I glycoprotein gH occurs through a cholesterol-dependent mechanism. *Soft Matter* **11**: 3003-16
53. Gianni T, Campadelli-Fiume G (2012) αVβ3-integrin relocalizes nectin1 and routes herpes simplex virus to lipid rafts. *J Virol* **86**: 2850-5
54. Campadelli-Fiume G, Poletti L, Dall'Olio F, Serafini-Cessi F (1982) Infectivity and glycoprotein processing of herpes simplex virus type 1 grown in a ricin-resistant cell line deficient in N-acetylglucosaminyl transferase I. *Journal of virology* **43**: 1061-71
55. Serafini-Cessi F, Dall'Olio F, Scannavini M, Campadelli-Fiume G (1983) Processing of herpes simplex virus-1 glycans in cells defective in glycosyl transferases of the Golgi system: relationship to cell fusion and virion egress. *Virology* **131**: 59-70
56. Teuton JR, Brandt CR (2007) Sialic acid on herpes simplex virus type 1 envelope glycoproteins is required for efficient infection of cells. *Journal of virology* **81**: 3731-9
57. Takamatsu S, Antonopoulos A, Ohtsubo K, Ditto D, Chiba Y, Le DT, Morris HR, Haslam SM, Dell A, Marth JD*, et al.* (2010) Physiological and glycomic characterization of N-acetylglucosaminyltransferase-IVa and -IVb double deficient mice. *Glycobiology* **20**: 485-97
58. Ohtsubo K, Takamatsu S, Minowa MT, Yoshida A, Takeuchi M, Marth JD (2005) Dietary and genetic control of glucose transporter 2 glycosylation promotes insulin secretion in suppressing diabetes. *Cell* **123**: 1307-21
59. Khoder-Agha F, Sosicka P, Escriva Conde M, Hassinen A, Glumoff T, Olczak M, Kellokumpu S (2019) N-acetylglucosaminyltransferases and nucleotide sugar transporters form multi-enzyme-multi-transporter assemblies in golgi membranes in vivo. *Cell Mol Life Sci*
60. Iversen MB, Reinert LS, Thomsen MK, Bagdonaite I, Nandakumar R, Cheshenko N, Prabakaran T, Vakhrushev SY, Krzyzowska M, Kratholm SK*, et al.* (2016) An innate antiviral pathway acting before interferons at epithelial surfaces. *Nature immunology* **17**: 150-8
61. Farnsworth A, Wisner TW, Webb M, Roller R, Cohen G, Eisenberg R, Johnson DC (2007) Herpes simplex virus glycoproteins gB and gH function in fusion between the virion envelope and the outer nuclear membrane. *Proc Natl Acad Sci U S A* **104**: 10187-92
62. Bagdonaite I, Norden R, Joshi HJ, King SL, Vakhrushev SY, Olofsson S, Wandall HH (2016) Global Mapping of O-Glycosylation of Varicella Zoster Virus, Human Cytomegalovirus, and Epstein-Barr Virus. *J Biol Chem* **291**: 12014-28

63. Lin E, Spear PG (2007) Random linker-insertion mutagenesis to identify functional domains of herpes simplex virus type 1 glycoprotein B. *Proc Natl Acad Sci U S A* **104**: 13140-5
64. Cooper RS, Heldwein EE (2015) Herpesvirus gB: A Finely Tuned Fusion Machine. *Viruses* **7**: 6552-69
65. Fan Q, Kopp SJ, Byskosh NC, Connolly SA, Longnecker R (2018) Natural Selection of Glycoprotein B Mutations That Rescue the Small-Plaque Phenotype of a Fusion-Impaired Herpes Simplex Virus Mutant. *mBio* **9**
66. Cooper RS, Georgieva ER, Borbat PP, Freed JH, Heldwein EE (2018) Structural basis for membrane anchoring and fusion regulation of the herpes simplex virus fusogen gB. *Nat Struct Mol Biol* **25**: 416-424
67. Loret S, Guay G, Lippé R (2008) Comprehensive characterization of extracellular herpes simplex virus type 1 virions. *J Virol* **82**: 8605-18
68. Marsden HS, Crombie IK, Subak-Sharpe JH (1976) Control of protein synthesis in herpesvirus-infected cells: analysis of the polypeptides induced by wild type and sixteen temperature-sensitive mutants of HSV strain 17. *J Gen Virol* **31**: 347-72
69. Guenalp A (1965) GROWTH AND CYTOPATHIC EFFECT OF RUBELLA VIRUS IN A LINE OF GREEN MONKEY KIDNEY CELLS. *Proc Soc Exp Biol Med* **118**: 85-90
70. Desai P, Person S (1998) Incorporation of the green fluorescent protein into the herpes simplex virus type 1 capsid. *J Virol* **72**: 7563-8
71. Narimatsu Y, Joshi HJ, Yang Z, Gomes C, Chen YH, Lorenzetti FC, Furukawa S, Schjoldager KT, Hansen L, Clausen H*, et al.* (2018) A validated gRNA library for CRISPR/Cas9 targeting of the human glycosyltransferase genome. *Glycobiology* **28**: 295-305
72. Doench JG, Fusi N, Sullender M, Hegde M, Vaimberg EW, Donovan KF, Smith I, Tothova Z, Wilen C, Orchard R*, et al.* (2016) Optimized sgRNA design to maximize activity and minimize off-target effects of CRISPR-Cas9. *Nat Biotechnol* **34**: 184-191
73. Ran FA, Hsu PD, Wright J, Agarwala V, Scott DA, Zhang F (2013) Genome engineering using the CRISPR-Cas9 system. *Nat Protoc* **8**: 2281-2308
74. Sanjana NE SO, Zhang F. (2014) Improved vectors and genome-wide libraries for CRISPR screening. *Nat Methods* **11**: 783-784
75. Ehrhardt C, Schmolke M, Matzke A, Knoblauch A, Will C, Wixler V, Ludwig S (2006) Polyethylenimine, a cost-effective transfection reagent. *Signal transduction Banner* **6**: 179-184
76. Yang Z, Steentoft C, Hauge C, Hansen L, Thomsen AL, Niola F, Vester-Christensen MB, Frodin M, Clausen H, Wandall HH*, et al.* (2015) Fast and sensitive detection of indels induced by precise gene targeting. *Nucleic acids research* **43**: e59
77. Kudelka MR, Antonopoulos A, Wang Y, Duong DM, Song X, Seyfried NT, Dell A, Haslam SM, Cummings RD, Ju T (2016) Cellular O-Glycome Reporter/Amplification to explore O-glycans of living cells. *Nat Methods* **13**: 81-6
78. Yang Z, Wang S, Halim A, Schulz MA, Frodin M, Rahman SH, Vester-Christensen MB, Behrens C, Kristensen C, Vakhrushev SY*, et al.* (2015) Engineered CHO cells for production of diverse, homogeneous glycoproteins. *Nat Biotechnol* **33**: 842-4
79. Dabelsteen S, Hercule P, Barron P, Rice M, Dorsainville G, Rheinwald JG (2009) Epithelial cells derived from human embryonic stem cells display p16INK4A senescence, hypermotility, and differentiation properties shared by many P63+ somatic cell types. *Stem cells (Dayton, Ohio)* **27**: 1388-99

80. Visalli RJ, Courtney RJ, Meyers C (1997) Infection and replication of herpes simplex virus type 1 in an organotypic epithelial culture system. *Virology* **230**: 236-43
81. Namvar L, Olofsson S, Bergstrom T, Lindh M (2005) Detection and typing of Herpes Simplex virus (HSV) in mucocutaneous samples by TaqMan PCR targeting a gB segment homologous for HSV types 1 and 2. *J Clin Microbiol* **43**: 2058-64
82. Sayers CL, Elliott G (2016) Herpes Simplex Virus 1 Enters Human Keratinocytes by a Nectin-1-Dependent, Rapid Plasma Membrane Fusion Pathway That Functions at Low Temperature. *J Virol* **90**: 10379-10389
83. Bergström T, Sjögren-Jansson E, Jeansson S, Lycke E (1992) Mapping neuroinvasiveness of the herpes simplex virus type 1 encephalitis-inducing strain 2762 by the use of monoclonal antibodies. *Mol Cell Probes* **6**: 41-9

**Figure legends**

**Figure 1. Human keratinocyte library for probing host-pathogen interplay. A** Common cell surface glycoconjugates are depicted, with investigated classes of glycans highlighted in boxes. Structures are drawn according to the symbol nomenclature for glycans (SNFG). The glycoengineered cell library was generated by knocking out genes involved in respective biosynthetic pathways using CRISPR/Cas9 and ZFN technologies. **B** N-glycoprofiling of cell lines harboring alterations in N-glycan synthesis. **C** O-glyprofiling of cell lines harboring alterations in O-glycan synthesis. **D-F** The array of cell lines was infected with MOI 10 of HSV-1 Syn17+, and viral titers (**D**) and viral DNA content (**E**) in the media were measured at 17 hpi. Particle to PFU ratio is also shown (**F**). Data is shown as WT-normalized mean +SEM of 3 independent experiments for each knock out (KO) cell line. One sample t test was used to evaluate differences from 1. FDR at 5 % was controlled by two-stage step-up method of Benjamini, Krieger and Yekutieli (* $q < 0.05$, ** $q < 0.01$, *** $q < 0.001$, **** $q < 0.0001$).

**Figure 2. Binding and entry of HSV-1 to mutant cell lines. A-C** 200 PFU of HSV-1 Syn17+ were allowed to adsorb to KO cell line monolayers for 20 min (**A**) or 120 min (**B**) on ice. Resulting plaques were quantified 48 h later. Data is shown as WT-normalized mean +SEM of 3 independent experiments for each KO cell line. One sample t test was used to evaluate differences from 1. FDR at 5 % was controlled by two-stage step-up method of Benjamini, Krieger and Yekutieli (* $q < 0.05$, ** $q < 0.01$, *** $q < 0.001$, **** $q < 0.0001$). **C** Proportion of virus bound at 20 min compared to 120 min is shown as mean +SEM of 3 independent experiments for each KO cell line. One-way ANOVA followed by Dunnett's multiple comparison test was used to evaluate differences from WT (* $p < 0.05$, ** $p < 0.01$, *** $p < 0.001$, **** $p < 0.0001$). **D-E** 200 PFU of HSV-1 Syn17+ were allowed to adsorb to KO cell line monolayers for 120 min on ice followed by 5 min warming to 37 °C and subsequent acid inactivation. Resulting plaques were quantified 48 h later. **D** Data is shown as WT-normalized mean +SEM of 3 independent experiments for each KO cell line. One sample t test was used to evaluate differences from 1. FDR at 5 % was controlled by two-stage step-up method of Benjamini, Krieger and Yekutieli (* $q < 0.05$, ** $q < 0.01$, *** $q < 0.001$, **** $q < 0.0001$). **E** Proportion of virus entered at 5 min compared to virus bound at 120 min is shown as mean +SEM of 3 independent experiments for each KO cell line. One-way ANOVA followed by Dunnett's multiple comparison test was used to evaluate differences from WT (* $p < 0.05$, ** $p < 0.01$, *** $p < 0.001$, **** $p < 0.0001$). **F** HaCaT WT and *B4GALT7* KO cells were probed for HSV-1

gC binding followed by mouse anti-gC and secondary antibodies. Heparinase 1, 2, and 3, chondroitinase ABC and combined treatments were included to evaluate contributions of HS and CS GAG chains. Scale bar: 10 µm. **G** The cartoon depicts a simplified overview of GAG synthesis. **H** A panel of CHO KO cell lines was used to measure HSV-1 gC binding followed by mouse anti-gC and secondary antibodies by flow cytometry. Control stainings omitted the gC probe and were used for subtracting background. Data is shown as WT-normalized geometrical mean +SEM of 3 independent experiments for each KO cell line. One sample t test was used to evaluate differences from 1. FDR at 5 % was controlled by two-stage step-up method of Benjamini, Krieger and Yekutieli (* $q < 0.05$, ** $q < 0.01$, *** $q < 0.001$, **** $q < 0.0001$).

**Figure 3. Viral assembly and properties of glycoengineered virions. A** HaCaT cells grown on cover slips were infected with MOI10 of HSV-1 K26-GFP and fixed and permeabilized at 14 hpi followed by co-staining for HSV-1 gD (magenta) and E-cadherin (cyan). Histograms on the left indicate intensities of gD and E-cadherin signals across the confocal images (marked with black arrowheads). Pixel overlap from the two channels is shown in white. GFP labelled capsid proteins (VP26) are seen in green. Nuclei were stained with DAPI (blue). Stainings of mock-infected cells are included. Scale bar: 10 µm. Images are representative of 2 independent experiments. **B** HaCaT cells grown on cover slips were infected with MOI10 of HSV-1 K26-GFP and fixed and permeabilized at 14 hpi followed by staining for HSV-1 gB (magenta). GFP labelled capsid proteins (VP26) are seen in green. Nuclei were stained with DAPI (blue). Scale bar: 10 µm. Magnified regions of merged images are indicated with dashed white boxes. Images are representative of 2 independent experiments. **C** HaCaT WT and *C1GALT1C1* KO cells were infected with MOI3 or MOI10 of HSV-1 K26-GFP and viral capsids imaged by live microscopy at 14 and 20 hpi. Fluorescent images overlaid with bright field images are also shown. Scale bar: 10 µm. **D-F** 200 PFU of HSV-1 Syn17+ produced in the different KO cell lines were allowed to adsorb to HaCaT WT monolayers for 20 min (**D**) or 120 min (**E**) on ice. Resulting plaques were quantified 48 h later. Data is shown as WT-normalized mean +SEM of 3 independent experiments for each glycoengineered virus species. One sample t test was used to evaluate differences from 1. FDR at 5 % was controlled by two-stage step-up method of Benjamini, Krieger and Yekutieli (* $q < 0.05$, ** $q < 0.01$, *** $q < 0.001$, **** $q < 0.0001$). **F** Proportion of virus bound at 20 min compared to 120 min is shown as mean +SEM of 3 independent experiments for each glycoengineered virus species. One-way ANOVA followed by Dunnett's multiple comparison test was used to evaluate differences from WT (* $p < 0.05$, ** $p < 0.01$, *** $p < 0.001$, **** $p < 0.0001$). **G-H** 200 PFU of HSV-1 Syn17+ produced in the different KO cell lines were allowed to adsorb to HaCaT WT monolayers for 120 min on ice followed by 5 min warming to 37 °C and subsequent acid inactivation. Resulting plaques were quantified 48 h later. **G** Data is shown as WT-normalized mean +SEM of 3 independent experiments for each glycoengineered virus species. One sample t test was used to evaluate differences from 1. FDR at 5 % was controlled by two-stage step-up method of Benjamini, Krieger and Yekutieli (* $q < 0.05$, ** $q < 0.01$, *** $q < 0.001$, **** $q < 0.0001$). **H** Proportion of virus entered at 5 min compared to virus bound at 120 min is shown as mean +SEM of 3 independent experiments for each glycoengineered virus species. One-way ANOVA followed by Dunnett's multiple comparison test was used to evaluate differences from WT (* $p < 0.05$, ** $p < 0.01$, *** $p < 0.001$, **** $p < 0.0001$).

**Figure 4. Single O-glycosites affect cell-cell fusion efficiency. A** HSV-1 gB structure (PDB: 2GUM) with select mutated O-glycan acceptor sites indicated within the dashed box. Respective previously identified O-glycans were drawn manually as yellow squares. Domains are numbered in roman numericals according to Heldwein *et al.*, Science 2006. **B** The cartoon illustrates the principle of split luciferase assay. **C** Cell surface expression of gB O-glycosite Thr to Ala mutants evaluated by CELISA using mouse anti-gB antibodies. Data is shown as mean absorbance at 450 nm +SD of three technical replicates and is representative of three independent experiments. **D-E** Cell-cell fusion activity over 240 min using gB O-glycosite Thr to Ala mutants. Data from two independent experiments is shown, where mean normalized luminescence of three technical replicates at each time point is indicated by a dot. Mean values of the two independent experiments are shown as thin lines. Data is normalized to maximum luminescence reading at final time point using WT gB for each experiment. The upper panel shows apparent measurements, whereas the values in the lower panel were adjusted to account for differences in cell surface expression of gB. **D** Data related to gB domain I mutations. **E** Data related to gB domain V mutations. **F** HSV-1 gD structure (PDB: 2C36) with select mutated O-glycan acceptor sites indicated. Positions after removal of signal peptide, often encountered in the literature, are indicated in brackets. Respective previously identified O-glycans were drawn manually as yellow squares. N-terminal region omitted in the crystal structure is drawn as a dashed line. **G** Cell surface expression of gD O-glycosite Thr to Ala mutants evaluated by CELISA using mouse anti-gD antibodies. Data is shown as mean absorbance at 450 nm +SD of three technical replicates and is representative of three independent experiments. **H** Cell-cell fusion activity over 240 min using gD O-glycosite Ser/Thr to Ala mutants. Data from two independent experiments is shown, where mean normalized luminescence of three technical replicates at each time point is indicated by a dot. Mean values of the two independent experiments are shown as thin lines. Data is normalized to maximum luminescence reading at final time point using WT gD for each experiment. The upper panel shows apparent measurements, whereas the values in the lower panel were adjusted to account for differences in cell surface expression of gD.

**Figure 5. HSV-1 cell-to-cell spread in mutant cell monolayers and cultured tissues. A** Plaque assay was used to evaluate 2D cell-to-cell spread in glycoengineered HaCaT cell monolayers, and organotypic skin model infections were used for inspecting 3D spread. **B** Plaque diameter on cell monolayers infected with HSV-1 Syn17+ at 48 hpi. Data is presented as violin diagrams that include measurements from 3 independent experiments for each KO cell line, with 50 plaques measured for each experiment. Paired WT data includes measurements from 15 independent experiments. The dashed lines within the plots indicate median diameter, whereas the dotted lines indicate the interquartile range. One-way ANOVA followed by Games-Howell's multiple comparison test was used to evaluate differences from WT (* $p < 0.05$, ** $p < 0.01$, *** $p < 0.001$, **** $p < 0.0001$). **C** Cell monolayers grown on large cover slips were infected with 200 PFU of HSV-1 K26-GFP and overlaid with semi-solid media for 48 h followed by fixation and staining for HSV-1 gE (red). GFP labelled capsid proteins (VP26) are seen in green. Confocal images at two different magnifications were taken to illustrate overviews of plaques (upper panels) as wells as gE expression at higher resolution (lower panels). Scale bars for the different magnifications are indicated. **D-G** Fully differentiated 3D skin models built with glycoengineered cells were infected with HSV-1 Syn17+ for 36 h followed by fixation in formalin and embedding in paraffin. **D** The cartoon illustrates the procedure for evaluating HSV-1 spread in organotypic skin tissues. FFPE

tissues were sectioned every 30 µm for 10 consecutive slices containing two sections each, spanning from the center of the tissue outwards in two directions. **E** Consecutive sections were stained with a polyclonal FITC-labelled anti-HSV-1 antibody to visualize virus lesions and whole sections imaged with a microscope slide scanner. An example section series is shown with HSV-1 lesions outlined in purple. **F** Representative lesions were selected from the scanned section series for each KO tissue. **G** Three lesions spanning several sections were identified for each KO tissue and lesion area measured at the centermost section. Data is shown as mean +SEM with individual measurement values indicated as black dots. One-way ANOVA followed by Dunnett's multiple comparison test was used to evaluate differences from WT (* $p < 0.05$, ** $p < 0.01$, *** $p < 0.001$, **** $p < 0.0001$).

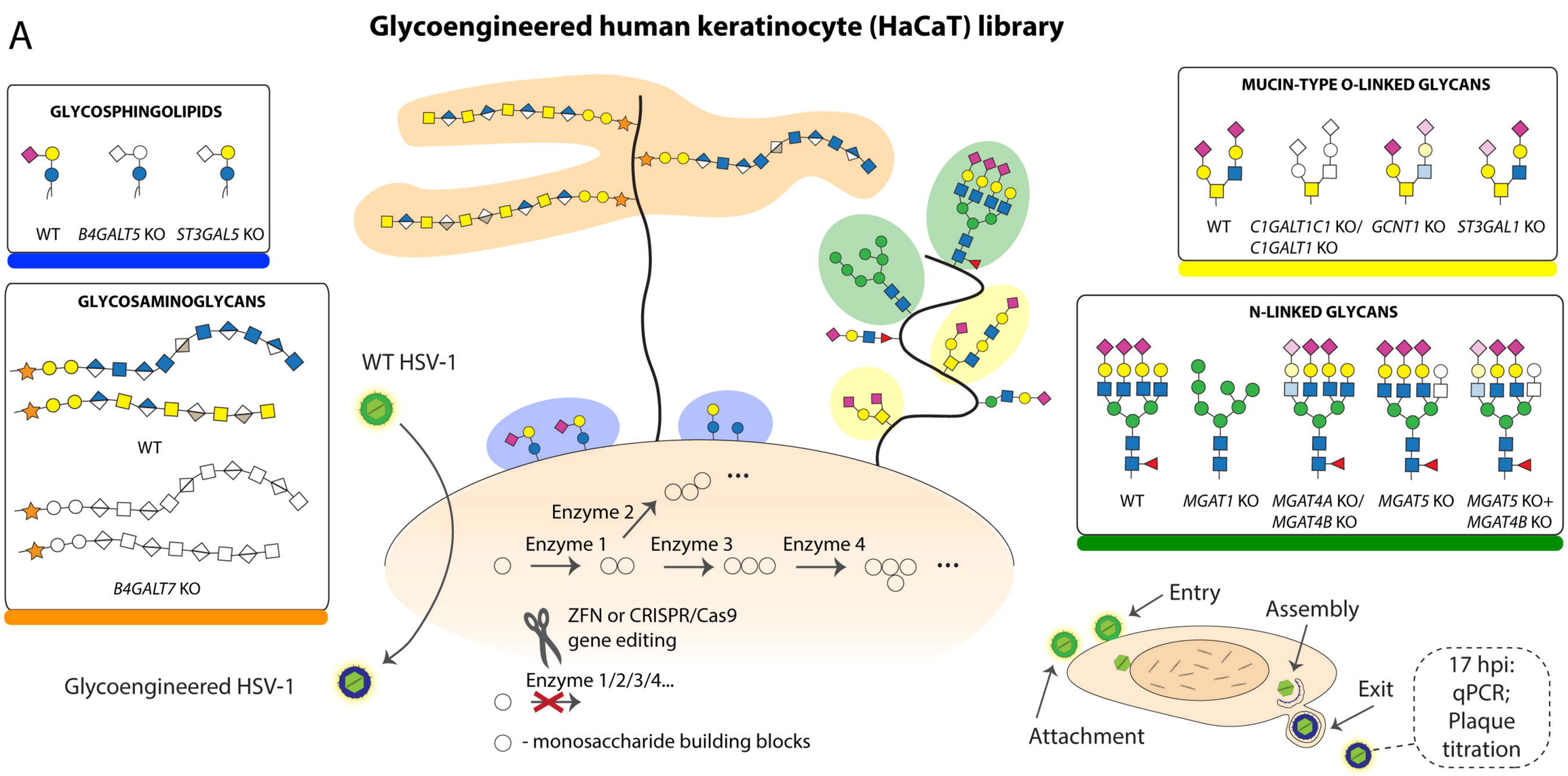
A
Glycoengineered human keratinocyte (HaCaT) library
GLYCOSPHINGOLIPIDS
WT
B4GALT5 KO
ST3GAL5 KO
GLYCOSAMINOGLYCANS
WT
B4GALT7 KO
WT HSV-1
Glycoengineered HSV-1
Enzyme 1
Enzyme 2
Enzyme 3
Enzyme 4
ZFN or CRISPR/Cas9 gene editing
Enzyme 1/2/3/4...
- monosaccharide building blocks
MUCIN-TYPE O-LINKED GLYCANS
WT
C1GALT1C1 KO/ C1GALT1 KO
GCNT1 KO
ST3GAL1 KO
N-LINKED GLYCANS
WT
MGAT1 KO
MGAT4A KO/ MGAT4B KO
MGAT5 KO
MGAT5 KO+ MGAT4B KO
Entry
Assembly
Exit
Attachment
17 hpi: qPCR; Plaque titration

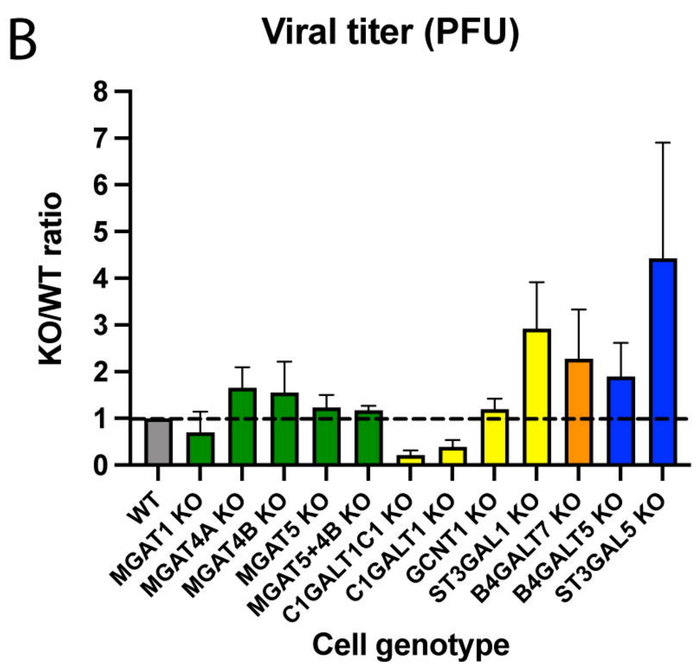
B
Viral titer (PFU)
KO/WT ratio
0
1
2
3
4
5
6
7
8
WT
MGAT1 KO
MGAT4A KO
MGAT4B KO
MGAT5 KO
MGAT5+4B KO
C1GALT1C1 KO
C1GALT1 KO
GCNT1 KO
ST3GAL1 KO
B4GALT7 KO
B4GALT5 KO
ST3GAL5 KO
Cell genotype

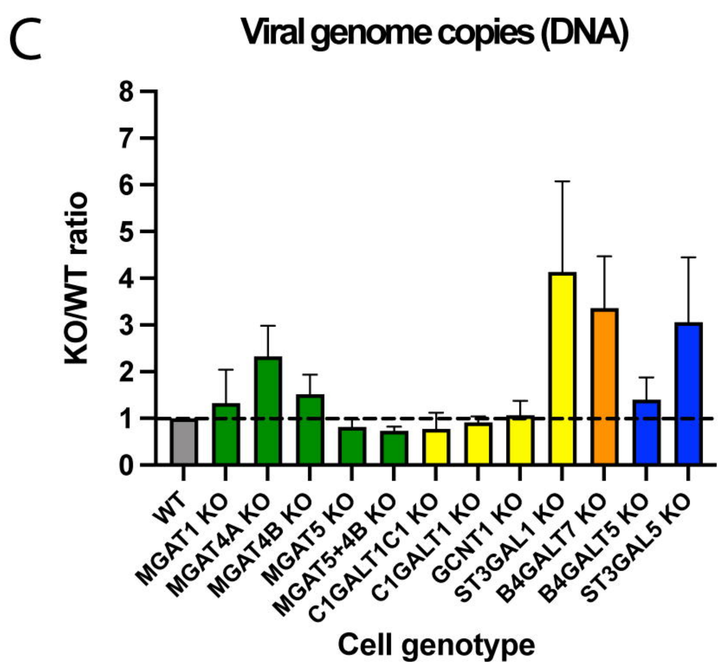
C
Viral genome copies (DNA)
KO/WT ratio
0
1
2
3
4
5
6
7
8
WT
MGAT1 KO
MGAT4A KO
MGAT4B KO
MGAT5 KO
MGAT5+4B KO
C1GALT1C1 KO
C1GALT1 KO
GCNT1 KO
ST3GAL1 KO
B4GALT7 KO
B4GALT5 KO
ST3GAL5 KO
Cell genotype

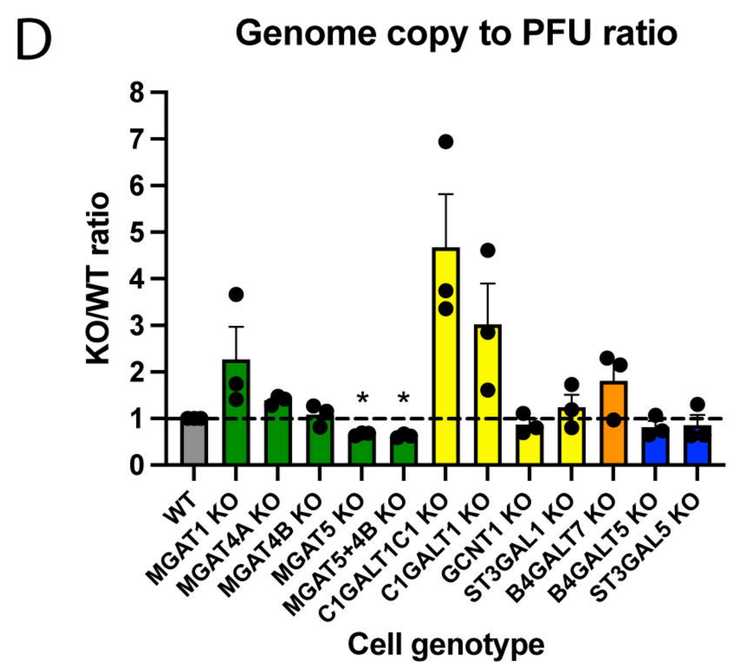
D
Genome copy to PFU ratio
KO/WT ratio
0
1
2
3
4
5
6
7
8
*
*
WT
MGAT1 KO
MGAT4A KO
MGAT4B KO
MGAT5 KO
MGAT5+4B KO
C1GALT1C1 KO
C1GALT1 KO
GCNT1 KO
ST3GAL1 KO
B4GALT7 KO
B4GALT5 KO
ST3GAL5 KO
Cell genotype

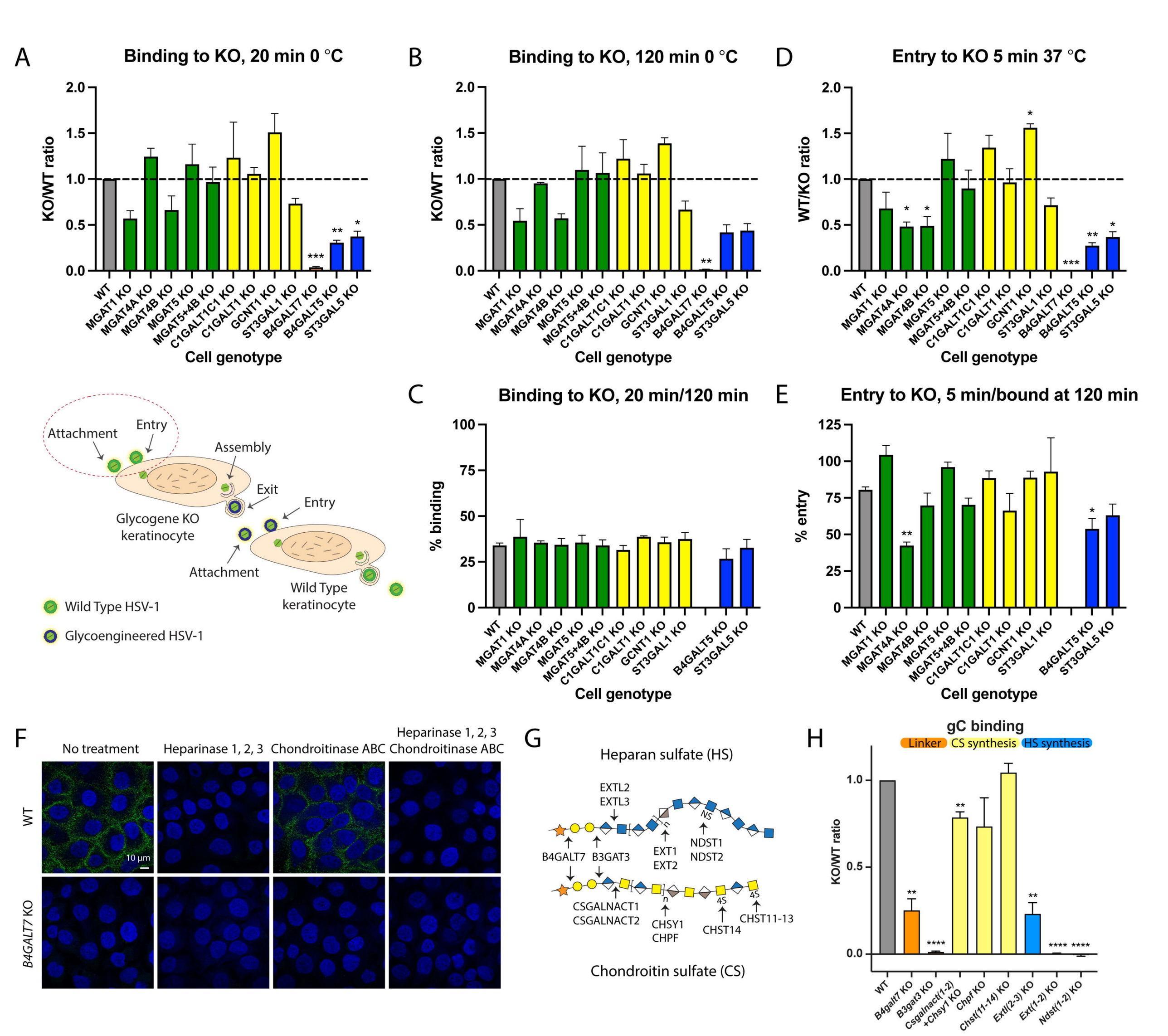
A
Binding to KO, 20 min 0 °C
KO/WT ratio
Cell genotype
B
Binding to KO, 120 min 0 °C
KO/WT ratio
Cell genotype
D
Entry to KO 5 min 37 °C
WT/KO ratio
Cell genotype
WT
MGAT1 KO
MGAT4A KO
MGAT4B KO
MGAT5 KO
MGAT5+4B KO
C1GALT1C1 KO
C1GALT1 KO
GCNT1 KO
ST3GAL1 KO
B4GALT7 KO
B4GALT5 KO
ST3GAL5 KO
Attachment
Entry
Assembly
Exit
Entry
Glycogene KO keratinocyte
Attachment
Wild Type keratinocyte
Wild Type HSV-1
Glycoengineered HSV-1
C
Binding to KO, 20 min/120 min
% binding
Cell genotype
E
Entry to KO, 5 min/bound at 120 min
% entry
Cell genotype
F
No treatment
Heparinase 1, 2, 3
Chondroitinase ABC
Heparinase 1, 2, 3 Chondroitinase ABC
WT
B4GALT7 KO
10 µm
G
Heparan sulfate (HS)
EXTL2
EXTL3
B4GALT7
B3GAT3
EXT1
EXT2
NDST1
NDST2
CSGALNACT1
CSGALNACT2
CHSY1
CHPF
CHST14
CHST11-13
Chondroitin sulfate (CS)
H
gC binding
Linker
CS synthesis
HS synthesis
KO/WT ratio
WT
B4galt7 KO
B3gat3 KO
Csgalnact(1-2) +Chsy1 KO
Chpf KO
Chst(11-14) KO
Extl(2-3) KO
Ext(1-2) KO
Ndst(1-2) KO

A

HSV-1 14 hpi | gD | E-cad | gD +E-cad | Max projection overlap | VP26 GFP | gD+E-cad +VP26 GFP | DAPI | Merge | Mock, merge

WT

*C1GALT1C1* KO

*C1GALT1* KO

*ST3GAL1* KO

*MGAT1* KO

B

gB | VP26 GFP | DAPI | Merge | Merge

WT

*C1GALT1C1* KO

*C1GALT1* KO

*ST3GAL1* KO

*MGAT1* KO

C

HSV-1 MOI 3, 14 hpi | HSV-1 MOI 10, 14 hpi | Mock, 14 hpi

VP26 GFP | GFP+BF | VP26 GFP | GFP+BF | GFP+BF

WT

*C1GALT1C1* KO

HSV-1 MOI 3, 20 hpi | HSV-1 MOI 10, 20 hpi | Mock, 20 hpi

VP26 GFP | GFP+BF | VP26 GFP | GFP+BF | GFP+BF

WT

*C1GALT1C1* KO

D

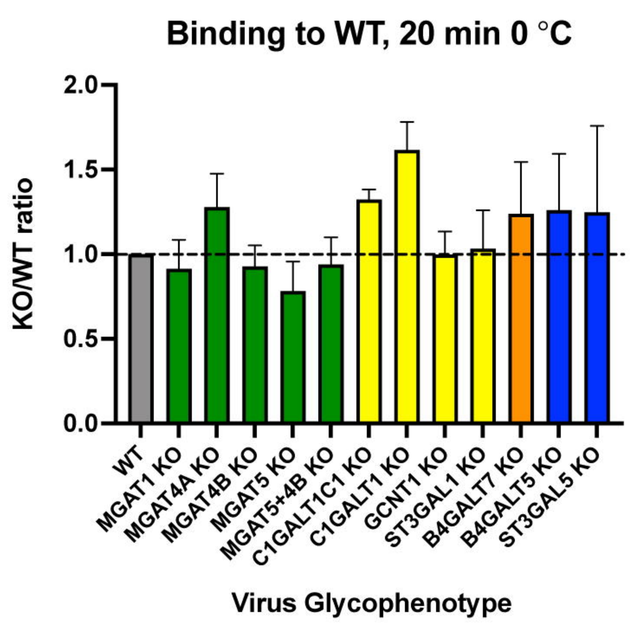


E

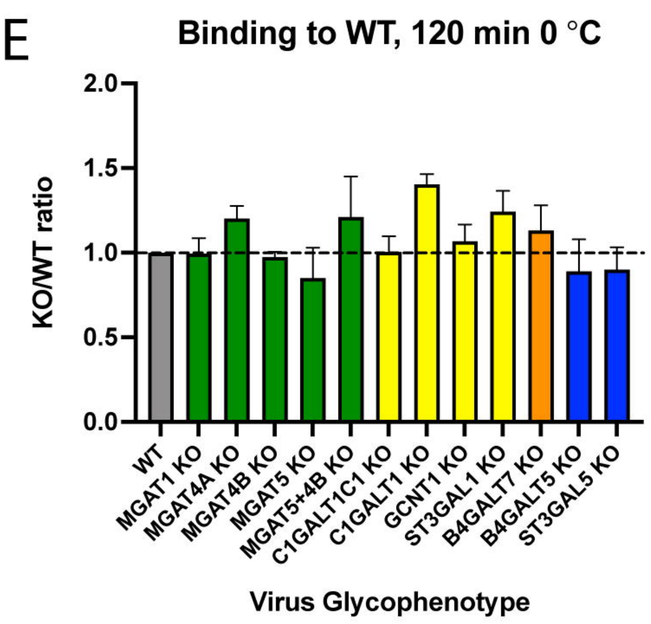


G

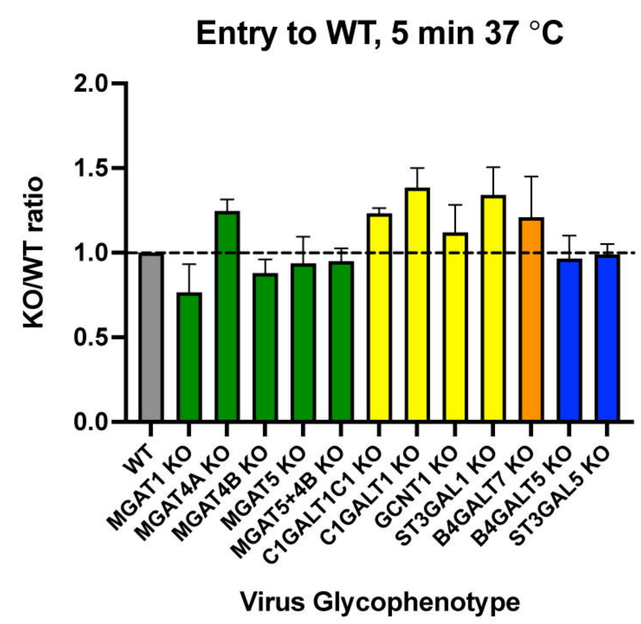


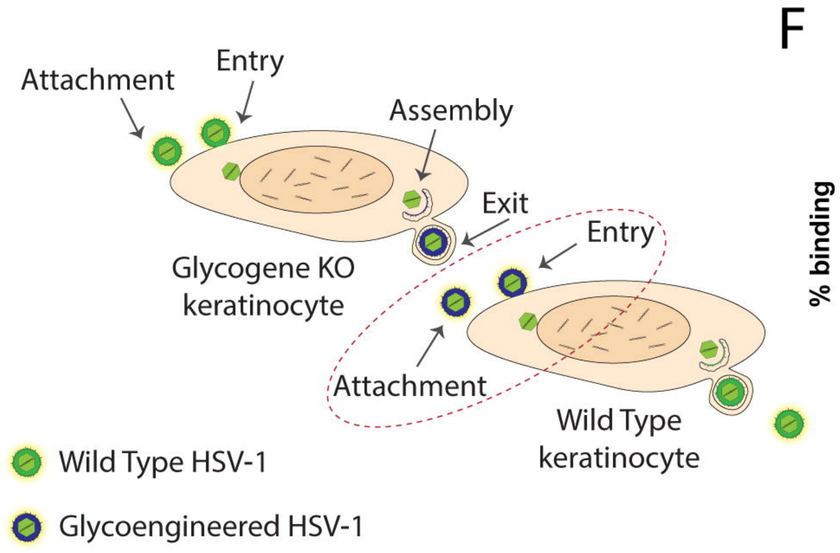


F

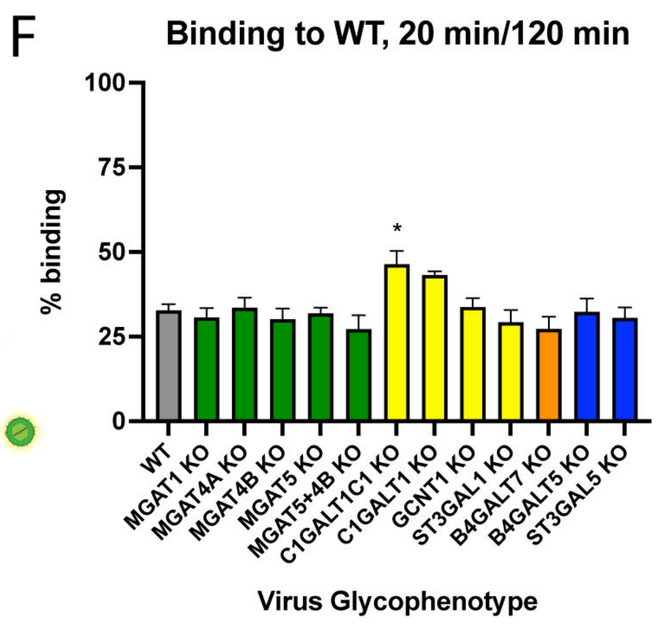


H

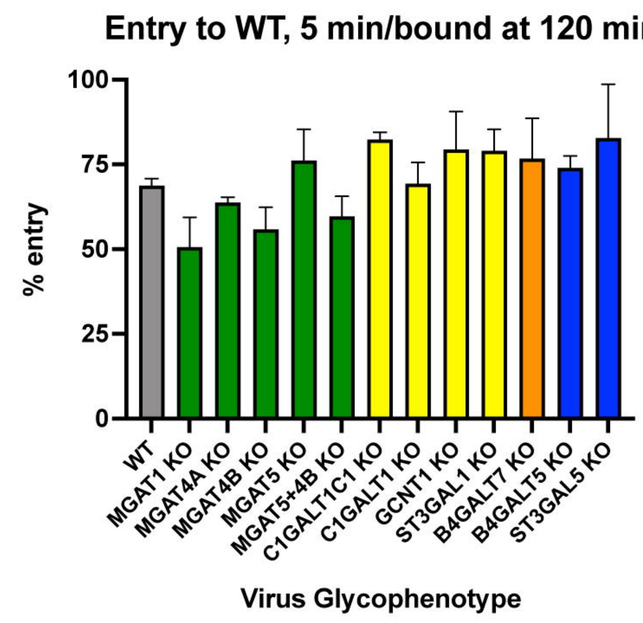

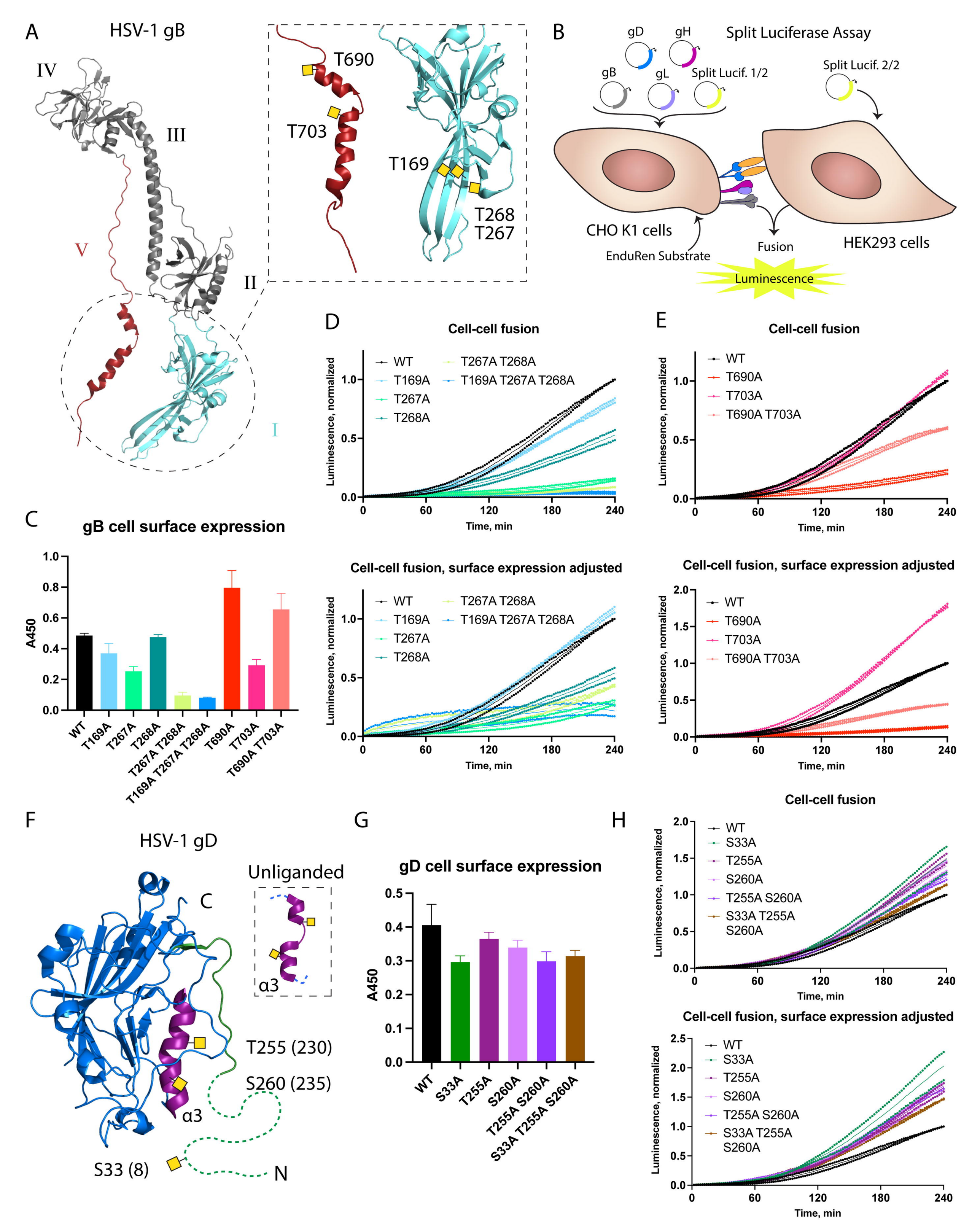
A
HSV-1 gB
IV
III
V
II
I
T690
T703
T169
T268
T267
B
Split Luciferase Assay
gD
gH
gB
gL
Split Lucif. 1/2
Split Lucif. 2/2
CHO K1 cells
EnduRen Substrate
Fusion
HEK293 cells
Luminescence
C
gB cell surface expression
A450
WT
T169A
T267A
T268A
T267A T268A
T169A T267A T268A
T690A
T703A
T690A T703A
D
Cell-cell fusion
Luminescence, normalized
Time, min
Cell-cell fusion, surface expression adjusted
E
Cell-cell fusion
Cell-cell fusion, surface expression adjusted
F
HSV-1 gD
Unliganded
C
α3
T255 (230)
S260 (235)
S33 (8)
N
G
gD cell surface expression
S33A
T255A
S260A
T255A S260A
S33A T255A S260A
H
Cell-cell fusion
Cell-cell fusion, surface expression adjusted

A

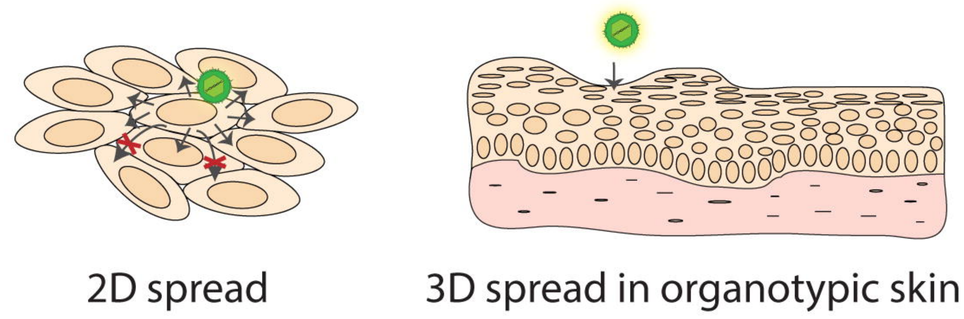
2D spread
3D spread in organotypic skin

B

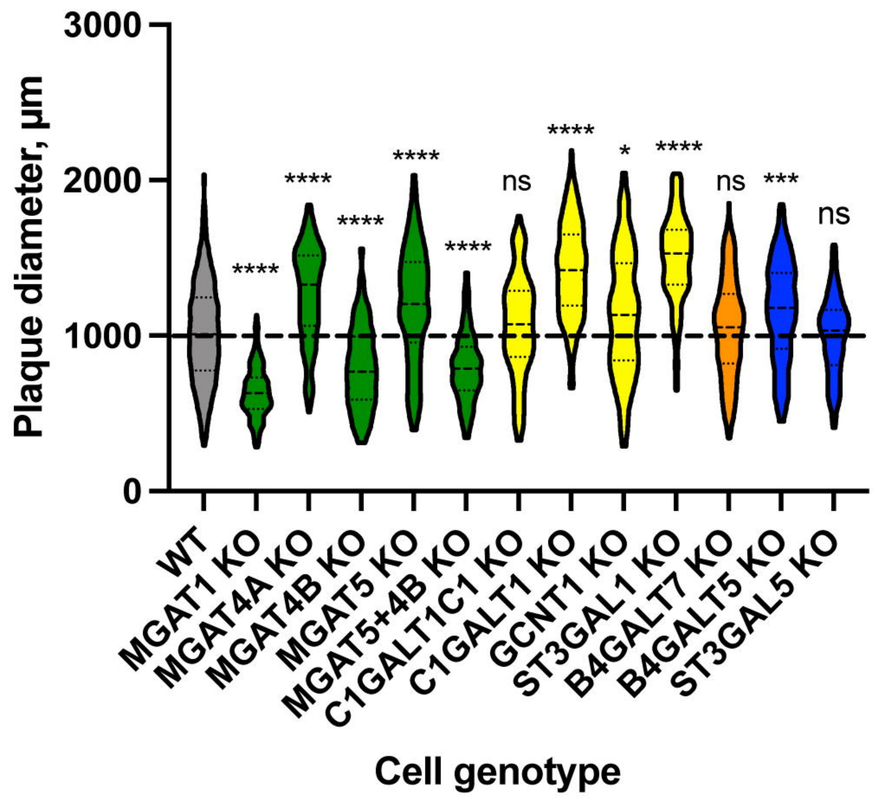
Plaque size distribution
Plaque diameter, µm
3000
2000
1000
0
****
****
****
****
****
ns
****
*
****
ns
***
ns
WT
MGAT1 KO
MGAT4A KO
MGAT4B KO
MGAT5 KO
MGAT5+4B KO
C1GALT1C1 KO
C1GALT1 KO
GCNT1 KO
ST3GAL1 KO
B4GALT7 KO
B4GALT5 KO
ST3GAL5 KO
Cell genotype

C

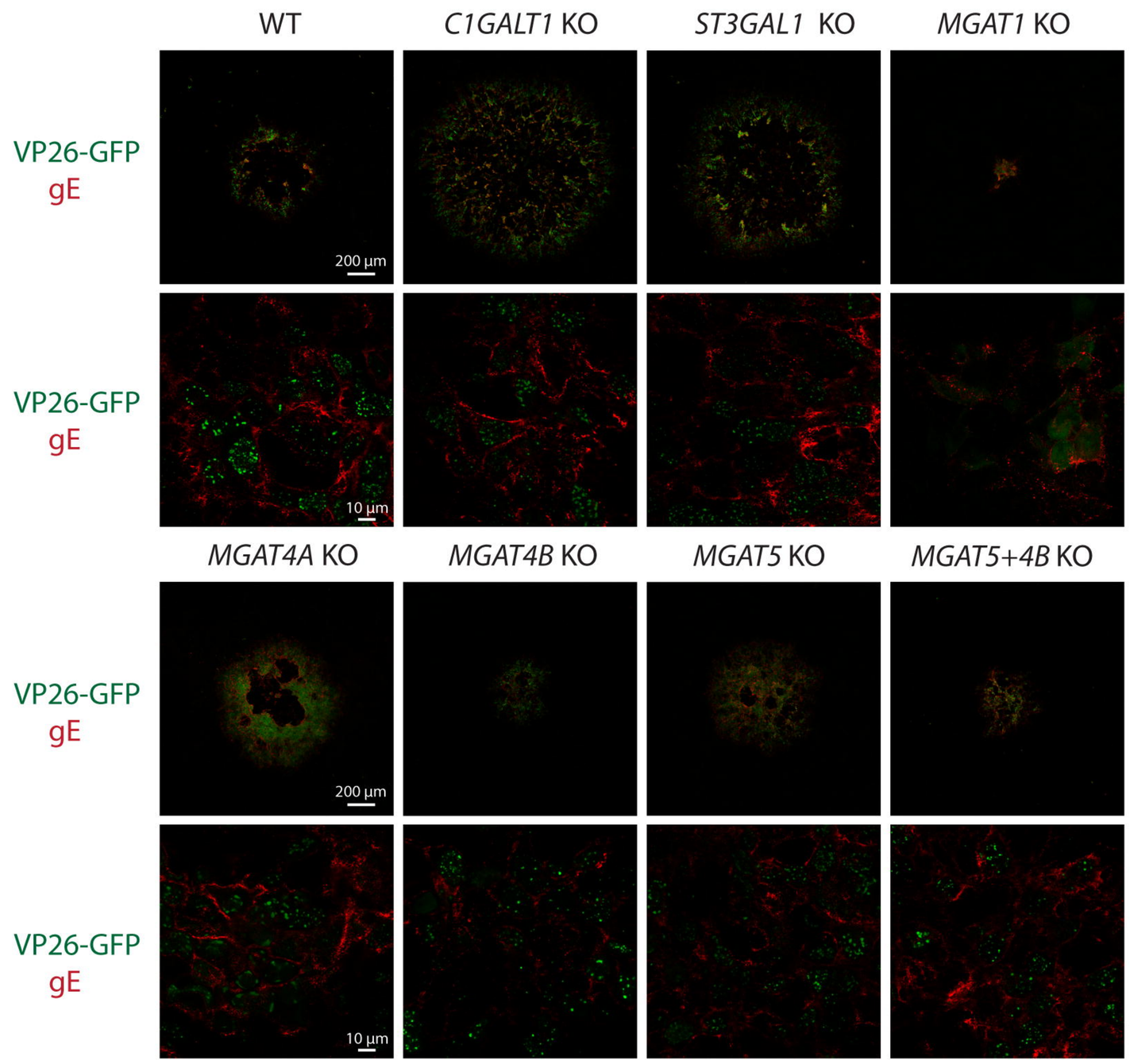
WT
C1GALT1 KO
ST3GAL1 KO
MGAT1 KO
VP26-GFP
gE
200 µm
10 µm
MGAT4A KO
MGAT4B KO
MGAT5 KO
MGAT5+4B KO

D

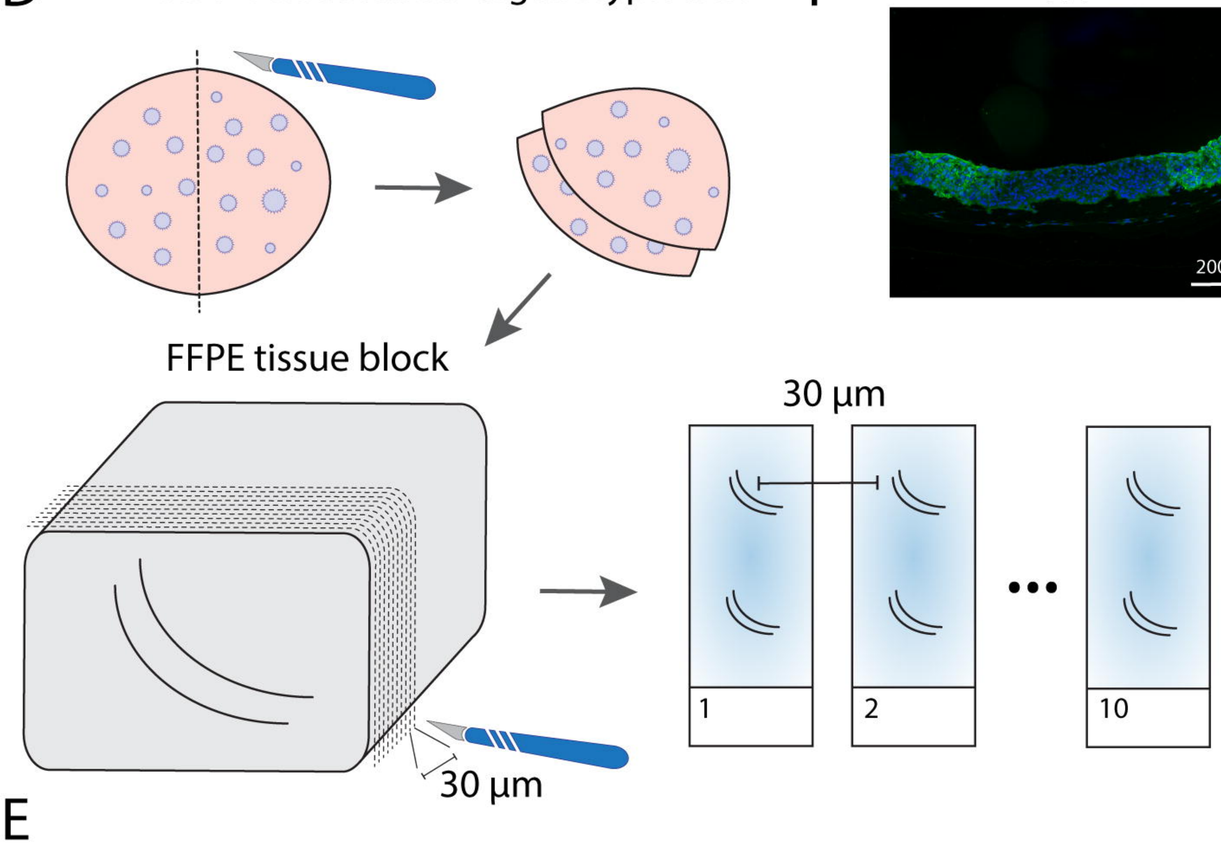
HSV-1-infected 3D organotypic skin
FFPE tissue block
30 µm
1
2
10
30 µm

E

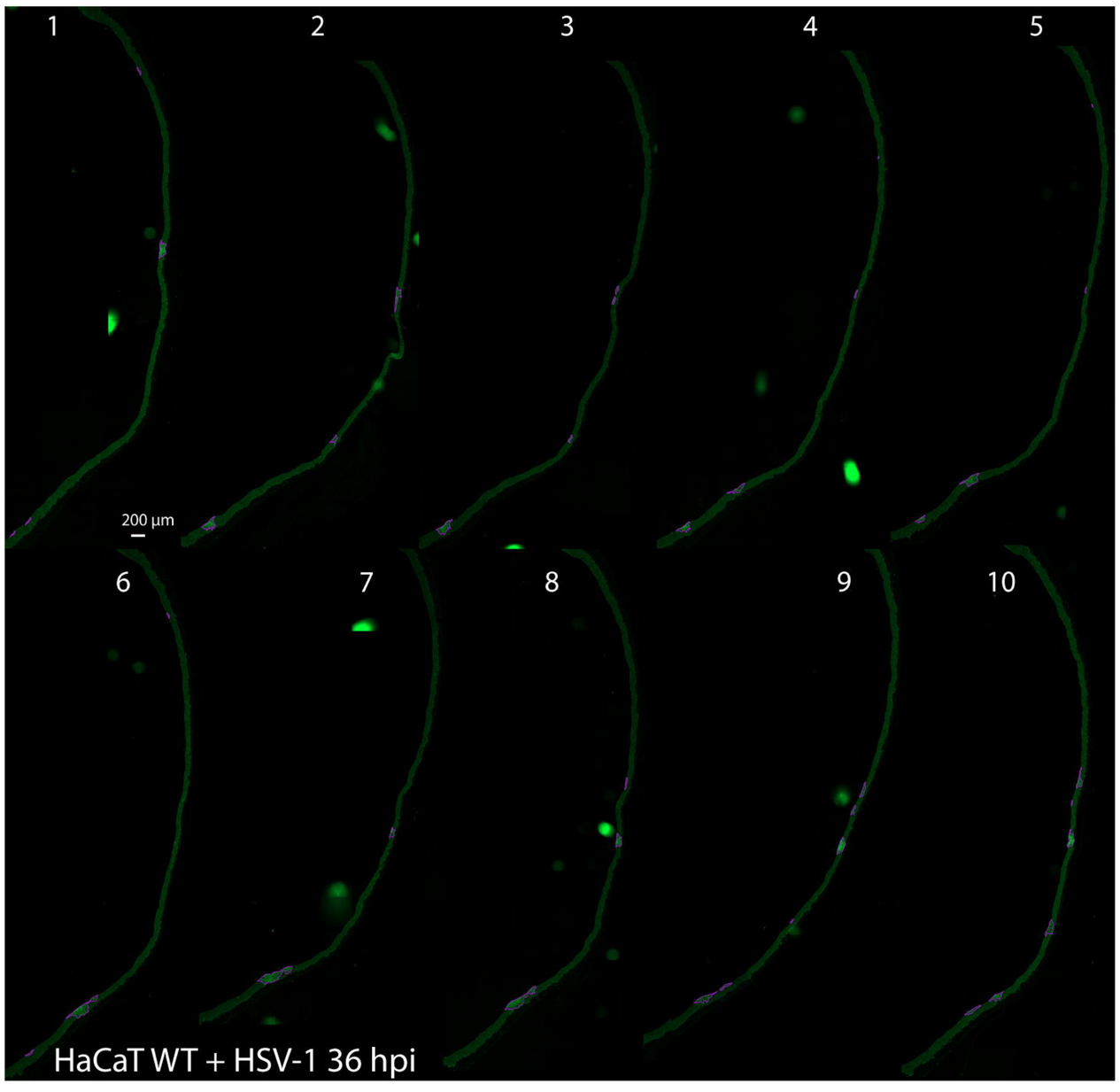
1
2
3
4
5
6
7
8
9
10
200 µm
HaCaT WT + HSV-1 36 hpi

F

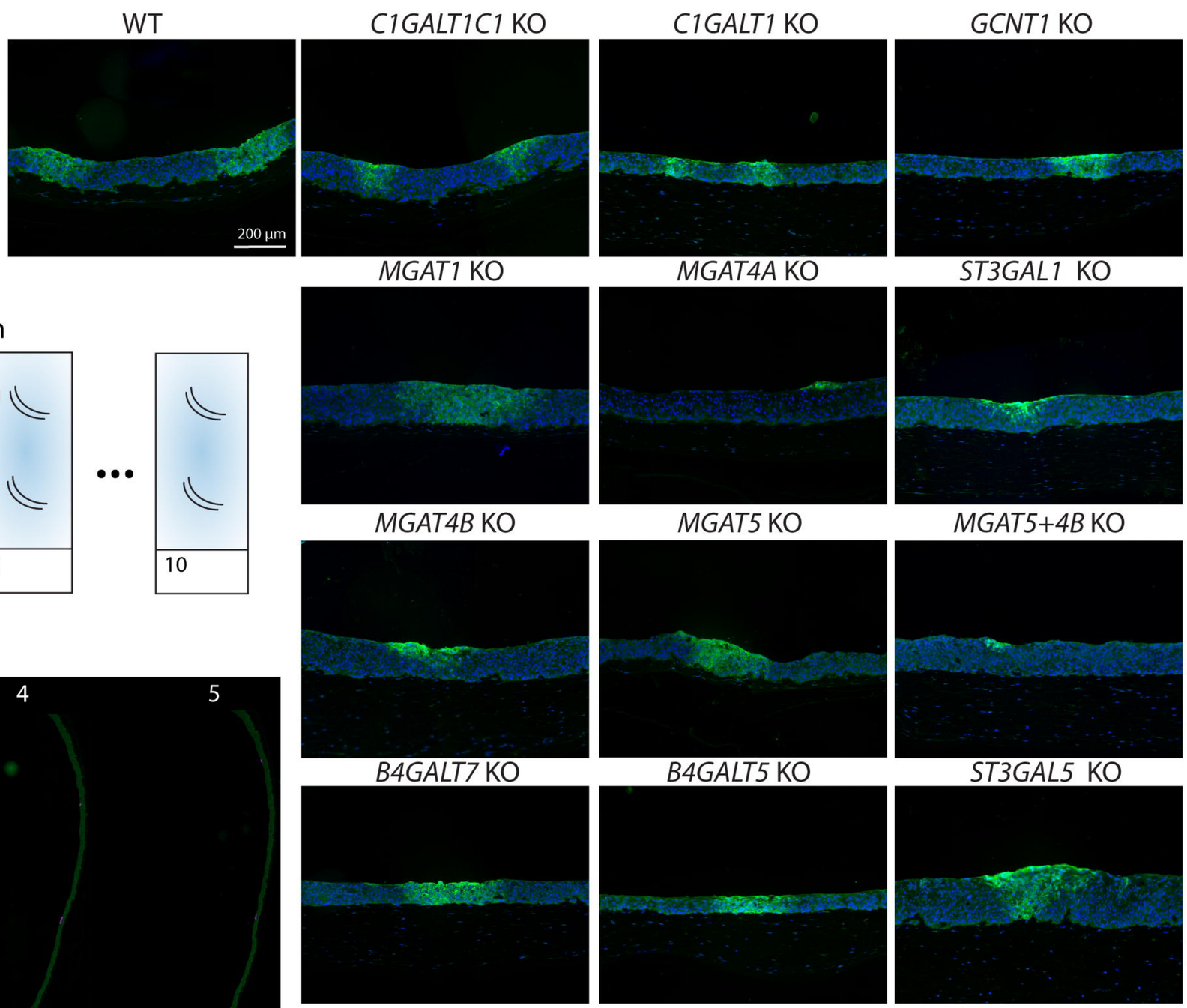
WT
C1GALT1C1 KO
C1GALT1 KO
GCNT1 KO
200 µm
MGAT1 KO
MGAT4A KO
ST3GAL1 KO
MGAT4B KO
MGAT5 KO
MGAT5+4B KO
B4GALT7 KO
B4GALT5 KO
ST3GAL5 KO

G

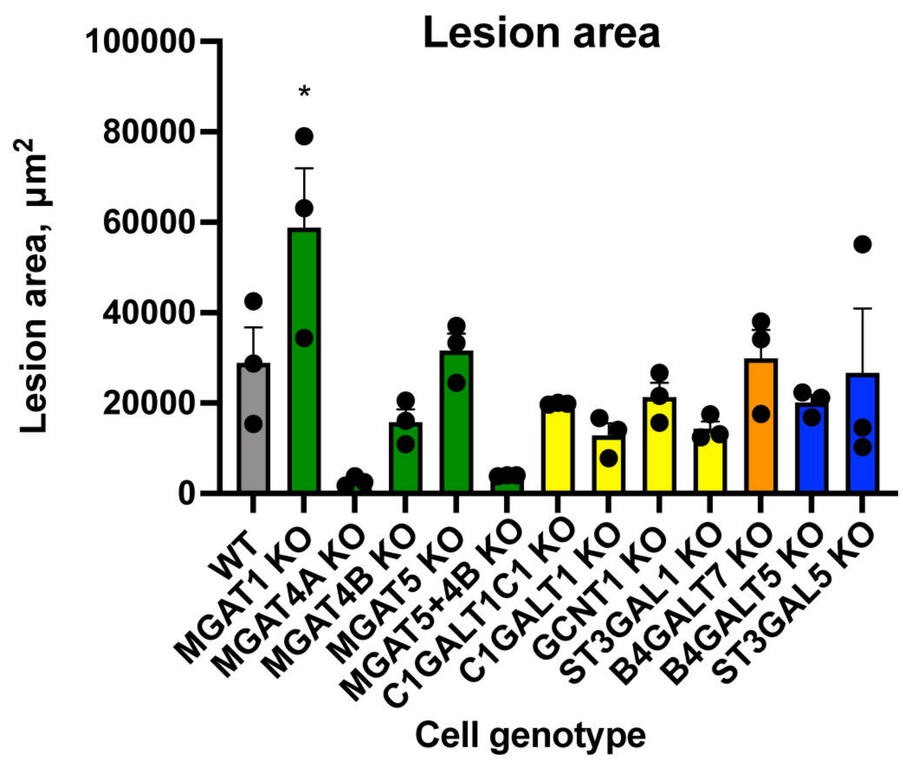
Lesion area
Lesion area, µm²
100000
80000
60000
40000
20000
0
*
WT
MGAT1 KO
MGAT4A KO
MGAT4B KO
MGAT5 KO
MGAT5+4B KO
C1GALT1C1 KO
C1GALT1 KO
GCNT1 KO
ST3GAL1 KO
B4GALT7 KO
B4GALT5 KO
ST3GAL5 KO
Cell genotype